An improved perspective in the spatial representation of soil moisture: potential added value of SMOS disaggregated 1 km resolution "all weather" product

Samiro Khodayar[1], Amparo Coll[2], Ernesto Lopez-Baeza[2]

[1] Institute of Meteorology and Climate Research (IMK-TRO), Karlsruhe Institute of

Technology (KIT), Karlsruhe, Germany

[2] University of Valencia, Spain. Earth Physics and Thermodynamics Department. Climatology

from Satellites Group

Submitted to HESS

* Corresponding author. E-mail address: samiro.khodayar@kit.edu (S. Khodayar)

Institute for Meteorology and Climate Research, Karlsruhe Institute of Technology (KIT),

Postfach 3640, 76021 Karlsruhe, Germany

1   **Abstract**

2   This study uses the synergy of multiresolution soil moisture (SM) satellite estimates from the

3   Soil Moisture Ocean Salinity (SMOS) mission, a dense network of ground-based SM

4   measurements, and a Soil Vegetation Atmosphere Transfer (SVAT) model, SURFEX

5   (Externalized Surface) – module ISBA (Interactions between Soil-Biosphere-Atmosphere), to

6   examine the benefits of the SMOS L4 version 3.0 or "all weather" high resolution soil

7   moisture disaggregated product (~ 1 km, SMOS_L4$^{3.0}$).   The added value compared to

8   SMOS-L3 (~ 25 km) and L2 (~15 km) is investigated. In situ SM observations over the

9   Valencia Anchor Station (VAS; SMOS Calibration/Validation (Cal/Val) site in Europe) are

10   used for comparison. The SURFEX(ISBA) model is used to simulate point-scale surface SM

11   (SSM) and, in combination with high-quality atmospheric information data, namely ECMWF

12   and the SAFRAN meteorological analysis system, to obtain a representative SSM mapping

13   over the VAS. The sensitivity to realistic initialization with SMOS_L4$^{3.0}$ to simulate the

14   spatial and temporal distribution of SSM is assessed. Results demonstrate: (a) all SMOS

15   products correctly capture the temporal patterns, but, the spatial patterns are not accurately

16   reproduced by the coarser resolutions probably in relation to the contrast with point-scale in

17   situ measurements. (b) The potential of SMOS-L4$^{3.0}$ product is pointed out to adequately

18   characterize SM spatio-temporal variability reflecting patterns consistent with intensive point

19   scale SSM samples on a daily time scale. The restricted temporal availability of this product

20   dictated by the revisit period of the SMOS satellite compromises the averaged SSM

21   representation for longer periods than a day. (c) A seasonal analysis points out improved

22   consistency during December-January-February and September-October-November in

23   contrast to significantly worse correlations in March-April-May (in relation to the growing

24   vegetation) and June-July-August (in relation to low SSM values < 0.1 m^3/m^3 and low spatial

25   variability). (d) The combined use of the SURFEX(ISBA) SVAT model with the SAFRAN

26 system, initialized with SMOS-L4$^{3.0}$ 1 km disaggregated data is proven to be a suitable tool to

27 produce regional SM maps with high accuracy which could be used as initial conditions for

28 model simulations, flood forecasting, crop monitoring and crop development strategies,

29 among others.

30 *Key Words: soil moisture, SMOS 1-km disaggregated product, SURFEX, Valencia Anchor*

31 *Station, realistic initialization, SAFRAN*

32

33

34

35

36

37

38

39

40

41

42

43

44

45

1. Introduction

Reliability of climate and hydrological models is constrained by associated uncertainties, such as input parameters. Among them, soil moisture is a variable of pivotal importance controlling the exchanges of water and energy at the surface/atmosphere interface (Entekhabi et al., 1996). Thus, it is a highly relevant variable for climate, hydrology, meteorology and related disciplines (e.g. Seneviratne et al. 2010).

Soil moisture is greatly variable spatially, temporally and across scales. The spatial heterogeneity of soil, vegetation, topography, land cover, rainfall and evapotranspiration are accounted responsible (Western et al., 2002; Bosh et al., 2007; Rosenbum et al. 2012).

The response of soil moisture to precipitation changes largely depends on soils water capacity and climatic zones. Particularly, in dry climates such as the Iberian Peninsula (IP), soil moisture quickly reacts to changes in precipitation (Li and Rodell 2013). Precipitation variability and mean are positively correlated, thus, an increase in precipitation yields wetter soils, which in turn results in higher spatial variability of soil moisture. An adequate representation of the high spatio-temporal variability of soil moisture is needed to improve climate and hydrological modelling (Koster et al., 2004; Seneviratne et al., 2006; Brocca et al., 2010). Its impact has been seen on time scales from hours to years (e.g., ~ 20 km scale: Taylor and Lebel, 1998; droughts: Schubert et al., 2004; decadal drying of the Sahel: Walker and Rowntree, 1977; hot extremes: Seneviratne et al., 2006b; Hirschi et al., 2011; decadal simulations: Khodayar et al., 2014). To obtain an appropriate representation of this variable, especially at high-resolution, is not an easy task mainly because of its high variability. Methods for the estimation of soil moisture can be divided in three main categories, (i) measurement of soil moisture in the field, (ii) estimation via simulation models, and (iii) measurement using remote sensing. In general, in situ measurements are far from global (e.g., Robock et al. 2000), and model simulations present important biases. Therefore, we have to

71 rely on space-borne sensors to provide such measurements, but until recent times no

72 dedicated, long-term, moisture space mission was attempted (Kerr, 2007).

73 Nowadays, by means of remote sensing technology surface soil moisture is available at global

74 scale (Wigneron et al., 2003). The best estimations result from microwave remote sensing at

75 low frequencies (e.g. Kerr, 2007; Jones et al., 2011) and several global soil moisture products

76 have been produced, such as the European Space Agency's Climate Change Initiative (ESA

77 CCI, Liu et al. 2011; Wagner et al. 2012) soil moisture products, the soil Moisture Active

78 Passive (SMAP; Entekhabi et al. 2010), the Advanced Microwave Scanning Radiometer-EOS

79 (AMSR-E; Owe et al. 2008), the advanced scatterometer (ASCAT; Naeimi et al. 2009) and

80 the Soil Moisture and Ocean Salinity (SMOS; Kerr et al., 2001) .

81 The SMOS mission is the first space-borne passive L-band microwave (1.4 GHz) radiometer

82 measuring at low frequency soil moisture over continental surfaces as well as ocean salinity

83 (Kerr et al., 2001, 2010). SMOS delivers global surface soil moisture measurements (~ 0-5

84 cm depth) at 0600 a.m. and 0600 p.m. LT (local time) in less than 3-days revisit at a spatial

85 resolution of ~ 44 km. The benchmark of the mission is to reach accuracy better than 0.04

86 m^3/m^3 for the provided global maps of soil moisture (Kerr et al., 2001).

87 SMOS data is not exempt of biases. Validating remote sensing-derived soil moisture products

88 is difficult, e.g. due to scale differences between the satellite footprints and the point

89 measurements on the ground (Cosh et al., 2004). However, in the last years a huge effort has

90 been made to validate the SMOS algorithm and its associated products. With this purpose, in

91 situ measurements across a range of climate regions were used assessing the reliability and

92 accuracy of these products using independent measurements (Delwart et al., 2008; Juglea et

93 al., 2010; Bircher et al., 2012; Dente et al., 2012; Gherboudj et al., 2012; Sánchez et al., 2012;

94 Wigneron et al., 2012). The strategy adapted by the European Space Agency (ESA) was to

95 develop specific land product validation activities over well-equipped monitoring sites. An

5

96   example for this is the Valencia Anchor Station (VAS; Lopez-Baeza et al., 2005a) in eastern

97   Spain, which was chosen as one of the two main test sites in Europe for the SMOS

98   Calibration/Validation (Cal/Val) activities. The validation sites were chosen to be slightly

99   larger than the actual pixel (3dB footprint), thus, VAS covers a 50x50 km^2 area. Within this

100   area, a limited number of ground stations were installed relying on spatialized soil moisture

101   information using the SVAT (Soil Vegetation Atmospheric Transfer) SURFEX (Externalized

102   Surface) model. Worldwide validation results reveal a coefficient of determination (R^2) of

103   about 0.49 when comparing the ~5 cm in situ soil moisture averages and the SMOS soil

104   moisture level 2 (SMOS-L2 ~ 15 km). For example, validation results by Bircher et al. (2012)

105   in Western Denmark show R^2 of 0.49-0.67 (SMOS retrieved initial soil moisture) and 0.97

106   (SMOS retrieved initial temperature). Besides, a significant under-/over-representation of the

107   network data (biases of – 0.092-0.057 m^3/m^3) is also found. Over the Maqu (China) and the

108   Twente (The Netherlands) regions, the validation analysis resulted in R^2 of 0.55 and 0.51,

109   respectively, for the ascending pass observations, and of 0.24 and 0.41, for the descending

110   pass observations. Furthermore, Dente et al. (2012) pointed out a systematic SMOS soil

111   moisture (ascending pass observations) dry bias of about 0.13 m^3/m^3 for the Maqu region and

112   0.17 m^3/m^3 for the Twente region. Validation of the SMOS level 3 product (SMOS-L3 ~ 35

113   km) shows that the general dry bias in SMOS-L2 is also present in SMOS-L3 SM. This bias

114   is markedly present in the ascending products and shorter time series as described in Sanchez

115   et al. (2012) and Gonzalez-Zamora et al. (2015). In this case, the presence of dense vegetation

116   is seen to increase RMSE scores, whereas in low vegetated areas a lower dry bias is found

117   (Louvet et al. 2015).

118   Since the launch of the SMOS satellite, the processing prototypes of the SMOS L2 soil

119   moisture have evolved, and their quality has improved. Furthermore, efforts have been made

120   to cover the need of a reliable product with finer resolution for hydrological and climatic

studies where the spatial variability of soil moisture plays a crucial role, e.g. in the estimation

of land surface fluxes (evapotranspiration (ET) and runoff). Piles et al. (2011) presented a

downscaling approach to optimally combine SMOS´ soil moisture estimates with MODIS

(Moderate Resolution Imaging Spectroradiometer) visible/infrared (VIS/IR) satellite data into

1 km soil moisture maps over the IP without significant degradation of the root mean square

error (RMSE). This product has been evaluated using the REMEDHUS (REd de MEDicion

de la HUmedad del Suelo) soil moisture network in the semi-arid area of the Duero basin,

Zamora, Spain (Piles et al. 2014). Results show that downscaling maintains temporal

correlation and root mean squared differences with ground-based measurements, hence,

capturing the soil moisture dynamics. Complementary studies after Piles et al. (2011) have

produced similar downscaled high-resolution SMOS-L4 soil moisture products (e.g.

Malbéteau et al (2018); Djamai et al (2016)). Being similar, however, the algorithms

originating them are totally different from those of SMOS-L4 used in this study. Whereas

SMOS-L4 products in this study proceed from the original SMOS-L2 (15 km resolution soil

moisture) disaggregated by 1-km MODIS LST and NDVI, Malbéteauet al (2018) and

Djamaiet al (2016) products proceed from the original SMOS-L1 (15 km resolution

brightness temperature).

A big limitation for the downscaling approach used in Piles et al. (2011) is the lack of

information in cloudy conditions of the hereafter named SMOS_L4$^{2.0}$, which significantly

limits the availability and usefulness of this product. In this study, we examine a new version

of the SMOS_L4 product, the SMOS Level 4 3.0 "all weather" disaggregated ~ 1 km SM

(SMOS_L4$^{3.0}$), which was developed and has been recently made available by SMOS-BEC

(Barcelona Expertise Centre).In this advanced high-resolution soil moisture product the

limitation on clouds is modulated by the use of ERA-Interim LST data, thus providing soil

moisture measurements independently of the cloud conditions.

146 Contrary toSMOS-L3 and -L2 products, which have been extensively validated as described

147 above and used for assimilation purposes in models (e.g. De Lannoy et al. 2016; Leroux et al.

148 2016), few studies deal with the disaggregated 1 km SMOS-L4$^{0.2}$ and SMOS-L4$^{0.3}$ products

149 (mostly in relation to wildfire activity) and validation efforts have concentrated only on the

150 REMEDHUS soil moisture network in Zamora (north-western Spain; e.g. Piles et al. 2014).

151 The objective of this paper is to provide information about the advantages and drawbacks and

152 the added value of the disaggregated 1 km SMOS-L4$^{3.0}$ "all weather" soil moisture product

153 with respect to coarser resolution products. The proposed investigation covers a one year

154 period (a complete hydrological cycle) and focuses on the semi-arid VAS area (eastern Spain)

155 and the IP where water availability and fire risk are big environmental issues, thus, knowledge

156 of soil moisture conditions is of pivotal importance. Furthermore, as spring time soil moisture

157 anomalies over the IP are believed to be a pre-cursor to droughts and heat waves in Europa

158 (Vautard et al. 2007; Zampieri et al. 2009), accurate monitoring and prediction of surface

159 states in this region may be key for improvements in seasonal forecasting systems.

160 The following objectives are then pursued: (a) Examination of soil moisture temporal and

161 spatial distribution with SMOS-derived soil moisture products over the investigation domain

162 using a multi-resolution approach: L3 (~ 25 km), L2 (~15 km), and L4$^{3.0}$ (~ 1 km), (b)

163 Validation with the in situ soil moisture measurements' network (VAS) to estimate the

164 reliability of the SMOS SM products, and (c) Evaluation of the impact of realistic SM

165 initialization using SMOS-L4$^{3.0}$ on point-scale and regional SURFEX(ISBA) model

166 simulations over the VAS area.

167 This investigation is structured as follows, in Section 2, the study area and the data sets are

168 presented including the in situ network measurements, the SMOS data products, and the

169 SURFEX(ISBA) model and related atmospheric forcings used. Section 3 summarizes the

170 methodology applied. The results are discussed in Section 4. Finally, conclusions are drawn in

171 Section 5.

172

173 **2. Study area and data set**

174 2.1 Investigation domain and in situ measurements over the VAS

175 The main investigation areas in this study are the Iberian Peninsula and the Valencia Anchor

176 Station (VAS) site located in eastern Spain (39.69°-39.22° N,-1.7°-(-1.11°) W). The VAS site

177 covering approximately a 50x50 km^2 area was established in December 2001 by the

178 University of Valencia as a Calibration/Validation (Cal/Val) site for different low-resolution

179 Earth Observation data products (Bolle et al., 2006). The extension and homogeneity of the

180 area as well as the mostly flat conditions (slopes lower than 2%) make it an ideal reference

181 site. Nevertheless, the small variations in the area, 750 to 950 m, influence the climate of the

182 region, which oscillates between semiarid to dry-sub-humid. Most of the area is dedicated to

183 vineyards (65%), followed by trees, shrubs, forest and industrial and urban cover types.

184 Mostly bare soil conditions are observed beside the vineyard growing season (March/April to

185 September/October). Mean temperatures in the region are between 12°C and 14°C with

186 annual mean precipitation about 450 mm, with maximums in spring and autumn. Within the

187 VAS, a network consisting of eight ThetaProbe ML2x soil moisture stations was deployed by

188 the Climatology from Satellites Group from the Earth Physics and Thermodynamics

189 Department at the University of Valencia. The eight in situ stations are distributed over a

190 10x10 km^2 area (Figure 1), according to land use, soil type, and other environmental

191 conditions. Details about the characteristics of each station are summarized in Table 1. Soil

192 moisture measurements every 10 min, mostly from 2006, were carried out for the top first 5

193 cm. More details about the VAS characteristics and soil moisture measurements could be

194 found in Juglea et al. (2010). Precipitation measurements over the IP and the VAS are from

195 the AEMET (Agencia Estatal de Meteorología; Spanish Weather Service) network.

196 Measurements every 10 min are available.

197 2.2 The SMOS surface soil moisture products

198 ESA's derived SMOS Soil Moisture Level 2 (SMOS-L2) data product, ~ 15 km, contains the

199 retrieved soil moisture and optical thickness and complementary parameters such as

200 atmospheric water vapour content, radio frequency interferences and other flags. The SMOS-

201 L2 algorithms have been refined since the launch of SMOS, resulting in more precise SM

202 retrievals (ARRAY, 2014). The Level 3 SM product, SMOS-L3, was obtained from the

203 operational CATDS archive. This is a daily product that contains filtered data. The best

204 estimation of SM is selected for each node when several multi-orbit retrievals are available

205 for a given day. A detection of particular events is also performed in order to flag the data.

206 The processing of the data separates morning and afternoon orbits. The aggregated products

207 are generated from this fundamental product. The Level 4 SM, SMOS-L4 2.0 data (SMOS-

208 L4$^{2.0}$), with 1 km spatial resolution is provided by BEC and covers the IP, Balearic Islands,

209 Portugal, South of France, and North of Morocco (latitudes 34°− 45° N and longitudes 10° W

210 − 5° E). A downscaling method that combines highly accurate, but low-resolution SMOS

211 radiometric information (SMOS-L2 data) with high-resolution (brightness temperature

212 measurements), but low sensitivity, visible-to-infrared imagery (NDVI (Normalized

213 Difference vegetation Index) and LST (Land Surface Temperature) from Aqua MODIS) to

214 SSM across spatial scales is used to derive the SMOS-L4$^{2.0}$ data (Piles et al 2010). The impact

215 of using different vegetation indices from MODIS with higher spatial and temporal resolution

216 in the downscaling method was explored in Sanchez-Ruiz et al. (2014), showing that the use

217 of more frequent and higher spatial-resolution vegetation information lead to improved SM

218 estimates. The latest SMOS-L4 product is the version 3.0 or "all weather" (SMOS-L4$^{3.0}$),

which is the product used and examined in this study. The downscaling approach is based on Piles et al. (2014) and Sanchez-Ruiz et al. (2014), with the novelty of introducing ERA-Interim LST data in the MODIS LST/NDVI scape, thus providing soil moisture measurements independently of the cloud conditions. ERA-Interim provides a resolution of about 0.125°, whereas MODIS is a ~ 1 km product. The evaluation of the SMOS-L4 2.0 and 3.0 products support the use of the "all weather" version, since it does not depend on cloud cover and the accuracy of the estimates with respect to in-situ data is improved or preserved (Piles et al. (2015), SMOS-BEC Team (2016)).

In this study, the SMOS-L2 V5.51 data coming from a L1C input product (obtained from MIRAS measurements), the SMOS-L3 V2.72 and the SMOS-L4 V3.0 are employed.

2.3 The SURFEX(ISBA) SVAT model

The SVAT model SURFEX (Externalized Surface, Le Moigne et al. 2009) − module ISBA (Interactions between Soil-Biosphere-Atmosphere, Noilhan and Planton 1989) is used to generate point-scale and spatially distributed SM spatial at 1 km grid spacing and temporal fields from initial conditions and atmospheric forcing. SURFEX(ISBA) was developed at the National Center for Metorological Research (CNRM), at Météo France, and it has been widely validated over vegetated and bare surfaces (e.g. Calvet et al. 1998). The ISBA scheme uses the Clapp and Hornberger (1978) soil water model and Darcy's law for the estimation of the diffusion of water in the soil, and allows 12 land use and related vegetation parameterization types. Crops are considered for the VAS area since mainly vineyards, almond and olive trees and shrubs compose the region.

The surface characteristics are considered in the SVAT input, roughness and the fraction of vegetation are adopted from ECOCLIMAP (Masson et al. 2003), topography is obtained from GTOPO (GTOPO30 Documentation) and soil types are defined using FAO (FAO, 2014).

243   To obtain an accurate simulation of soil moisture in the study area, the model was originally

244   calibrated by Juglea et al. (2010) to be applied over the entire site for any season/year.

245   Particularly relevant for this study is the specific definition of the soil hydraulic parameters

246   which they made for the VAS area, since most of the hydrological parameters are site

247   dependent and not available from SMOS observations. A new set of empirical equations as a

248   function of the percentages of sand and clay was defined using Cosby et al. (1984) and Boone

249   et al. (1999). New definitions and recommendations by Juglea et al. (2010) for the VAS area

250   were adopted in this investigation.

251   *Atmospheric forcing information: ECMWF and SAFRAN*

252   High quality atmospheric forcing is needed to carry out accurate simulations. To run the

253   SURFEX(ISBA) model, the following atmospheric forcing data are needed: air temperature

254   and humidity at screen level, atmospheric pressure, precipitation, wind speed and direction

255   and solar and atmospheric radiation. Three different sets of atmospheric forcing information

256   are used in this study as input forcing for the SURFEX(ISBA) simulations; (a) SURFEX-

257   OBS: meteorological data from 3 fully equipped stations in the OBS area, MELBEX-I,

258   MELBEX-II and VAS, (b) SURFEX-ECMWF: ECMWF (European Centre for Medium-

259   Range Weather Forecast) data, and (c) SURFEX-SAFRAN: information from the SAFRAN

260   (Système d'Analyse Fournissant des Renseignements Atmosphériques à la Neige)

261   meteorological analysis system (Durand et al. 1999; Quintana-Seguí et al. 2008; Vidal et al.

262   2010).

263   Precipitation, air temperature, surface pressure, air specific humidity, wind speed and

264   direction, downward longwave radiation, diffuse shortwave radiation, downward direct

265   shortwave radiation, snowfall rate and CO_2 concentration are used as input data from the

266   meteorological stations aforementioned in the OBS area. A temporal resolution of 10 min is

267   available. From ECMWF, dew point and temperature at 2 m, pressure, precipitation and wind

268 components, are used as forcing data, with a 6 h temporal resolution and 0.125°x0.125°

269 spatial resolution. Precipitation, air temperature, surface pressure, air specific humidity, wind

270 speed and downward shortwave and longwave radiation from SAFRAN are used as input

271 information with a spatial resolution of 8x8 km^2 and an hourly temporal resolution. In this last

272 case, we have an optimal spatial and temporal distribution of the atmospheric forcing over the

273 VAS area (~ 50x50 km^2) and a rare to find complete database to force the land surface model.

274 More details about the SAFRAN system and its validation in north-eastern Spain could be

275 found in Quintana-Seguí et al. (2016).

276

277 **3. Analysis methodology**

278 In order to investigate the characteristics and potential added values of fine-scale SMOS-

279 derived soil moisture, the spatial variability, the temporal evolution as well as the probability

280 distribution is investigated. With this purpose, SMOS-derived soil moisture products at

281 different spatial resolutions, in situ measurements and model simulations are jointly

282 evaluated.

283 The spatial distribution and temporal evolution of precipitation and SMOS-derived soil

284 moisture over the IP and the VAS area are assessed for the time period from December 2011

285 to December 2012 considering also hydrological seasons (DJF: December-January-February,

286 MAM: March-April-May, JJA: June-July-August, SON: September-October-November).

287 Special attention is paid to the autumn season since in this period the western Mediterranean

288 is characterized by a large thermal gradient between the atmosphere and the sea (Duffourg

289 and Ducrocq, 2011, 2013) resulting in intense precipitation extremes (Raveh-Rubin and

290 Wernli 2015). Furthermore, during 2012, the Hydrological Cycle in the Mediterranean

291 Experiment (HyMeX; Dobrinski et al. 2014) took place in the Western Mediterranean with

the IP and particularly the Valencia region as target areas. During the SON period of 2012, the Special Observation Period (SOP1; Ducrocq et al. 2014) with intensive experimental deployment over the area took place. This provides us with valuable information about the environmental conditions as well as the occurrence of precipitation events in the investigation area. Particularly, precipitation in the IP during the autumn (SON) period of 2012 was above average (Khodayar et al. 2015). It was also the hydrological season in which higher variability in the soil moisture was observed as a result of the precipitation distribution. Two unique events, at the end of September (27-29) affecting south and eastern Spain and at the end of November (19-20) affecting the Ebro valley (Jansà et al. 2014), largely determined the positive anomaly in precipitation and soil moisture in this period.

SMOS-L3 (~ 25 km), SMOS-L2 (~ 15 km), and SMOS-L4$^{3.0}$ (~ 1km) are used for the evaluation of soil moisture distribution at different grid spacing. Piles et al. (2014) pointed out that differences may exist between SMOS-L3–L2 and the 1 km disaggregated soil moisture SMOS-L4 because of the distinct methodology used to obtain these products. Only SMOS descending passes or a mean between ascendant and descent passes are used to calculate mean daily values of SMOS-derived soil moisture. Soil moisture derived from the afternoon orbits was found to be more accurate than the morning passes (Piles et al. 2014). The fine temporal resolution of the model simulations (1 h) and the observations (10 min) allow comparisons at the time of the SMOS overpasses. Because of the 3-day revisit period of the SMOS swath, the IP will not be fully covered by the satellite on daily basis. However, despite identified difficulties (radio frequency interferences, missing data ...), the IP is well observed being 1.5 days the average observations frequency over the IP. Only those images with coverage higher than 50% are considered in our calculations. A conservative remapping to coarser resolutions is applied, when required, to make comparisons among each other or with respect to ground-based observations on equal terms. Remapping allows point to point

317 comparisons between these data sets. In addition to the yearly and seasonal approach, an

318 exemplary short time period, 19 to 20 October of 2012, is considered. This corresponds to one

319 of the periods in which an extreme precipitation event occurred in the Ebro valley (at the end

320 of November; Jansà et al. 2014. Therefore, high variability in the soil moisture distribution is

321 expected.

322 The coefficient of variation (CV), defined as the ratio of the standard deviation to the mean,

323 of the precipitation and soil moisture fields over the IP, the VAS (50x50 km2) and the OBS

324 (10x10 km2) area are examined for the analysis of the spatial variability and its evolution in

325 time. The soil moisture daily index ($SM_{index,i}$) is calculated to assess the evolution pattern

326 allowing the study of daily variations

327 $SM_{index,i} = (SM_{i+1} - SM_i)/ SM_i$, where SM_{i+1} is the soil moisture of the day i+1 and SM_i is the

328 soil moisture of the day before i.

329 For these calculations, SMOS afternoon (descendant; Piles et al. 2014) orbits are selected as

330 well as observations at the time of the SMOS overpasses. For the IP and VAS, SMOS-L2 and

331 SMOS–L4$^{3.0}$ have been remapped to the coarser grid spacing for an adequate comparison.

332 Ground-based observations are aggregated using a mean over all stations for comparison with

333 the corresponding SMOS-L4$^{3.0}$ data (the closest grid point is selected).

334 The reliability of SMOS-L3, SMOS-L2 and SMOS-L4$^{3.0}$ soil moisture products is evaluated

335 by comparison with in situ soil moisture measurements in the OBS area. The spatial and

336 temporal variability are considered as well as the probability distribution. Different

337 approaches are applied: (a) the nearest grid point is selected for point-like comparisons

338 between SMOS-L2 and SMOS-L4$^{3.0}$ against in situ soil moisture stations, to reduce sampling

339 biases in this region of diverse soil characteristics (Table 1), (b) SMOS-L4$^{3.0}$ soil moisture

340 grid cells are averaged over the 10x10 km^2 area and compared to the mean from the soil

341   moisture network stations to address the issue related to spatial averaging due to the high

342   spatial and temporal variability of the upper-most SSM. For the comparison between the

343   SMOS-L2 and the in situ observations: when single ground-based stations are considered the

344   closest SMOS pixel is selected, in case of considering the OBS (10x10 km^2) or VAS (50x50

345   km^2) areas the mean over all pixels which centre falls within the area is used. For the

346   comparison with SMOS descending passes the corresponding values from in situ

347   measurements are considered. Additionally, a separation between wet days (precipitation over

348   1 mm/d) and dry days is applied to consider possible implications of wet/dry soils for SMOS

349   measurements.

350   Linear regression, the coefficient of determination (R^2), the mean bias (MB), and the root

351   mean square deviation (RMSD) are used to predefine the accuracy. A debiased or centred

352   RMSD (CRMSD) is applied to discriminate the systematic and random error components

353   removing the overall bias before calculating the RMSD.

354   Soil moisture modeling is performed by the use of the SVAT, SURFEX (Externalized

355   Surface) – module ISBA (Interactions between Soil-Biosphere-Atmosphere) from Météo-

356   France. Configuration and specifications described in Juglea et al. (2010), which proved

357   successful in adequately simulate the associated soil moisture heterogeneity over the wide

358   VAS surface (50x50 km^2), are adapted in this study. Simulations start on 1 December 2011 at

359   00UTC and cover the whole investigation period until 31 December 2012 with an hourly-

360   output time resolution. Point-scale SURFEX(ISBA) simulations over the soil moisture

361   network stations in the VAS domain are validated with the in situ measurements to assess the

362   usefulness of the model for further investigation, picturing the potential of the model in

363   simulating upper level soil moisture variability on different soil characteristics (Table 1).

364   To try to simulate the spatial and temporal heterogeneity of the soil moisture fields over the

365   VAS surface, the SURFEX(ISBA) scheme is used in combination with high quality forcing

366   data from ECMWF (hereafter SURFEX-ECMWF) and the SAFRAN system (hereafter

367   SURFEX-SAFRAN) for spatialization purposes. Soil moisture initialization in spatialized

368   SURFEX(ISBA) simulations requires a single representative value for the whole simulation

369   area. The benefit of initializing the simulations with SMOS-L4$^{3.0}$ data in comparison to

370   climatological means is discussed. In-situ soil moisture observations over the VAS area are

371   considered for verification. A comparison between SURFEX-SAFRAN point-scale and 10x10

372   km^2 mean simulations initialized with SMOS-L4$^{3.0}$ data is done against ground measurements

373   to assess the accuracy of the simulated SSM maps.

374

375   **4. Results**

376   4.1 SMOS-derived soil moisture at different resolutions

377   4.1.1 Spatial variability on seasonal and sub-seasonal time scales

378   Figure 2a shows the north-south precipitation gradient for the SON period mean. The SSM

379   satisfactorily reflects this gradient (Figure 2b), but, more markedly for the SMOS-L3 and

380   SMOS-L2 than the higher resolution SMOS-L4$^{3.0}$ showing lower standard deviation, SMOS-

381   L3(~0.15±0.01), SMOS-L2(~0.17±0.01), SMOS-L4(~0.22±0.007). The same performance is

382   seen over the VAS domain (not shown). The SSM variability associated to the extreme

383   precipitation events in this period is not well represented in the SMOS-L4$^{3.0}$ seasonal mean.

384   Table 2 shows the number of days (percentage) in which there is more than 50 % of data over

385   the IP for each SMOS product. These periods have been used as basis for the calculation of

386   the spatial distributions in Figure 2b. SMOS-L3 (88 %) and SMOS-L2 (84 %) show a good

387   coverage and similar number of days. However, a large difference is observed with respect to

388   the SMOS-L4$^{2.0}$ product with only 28 days (32 %) of adequate coverage for the period of

389   SON 2012. This is due to the problematic associated to the downscaling approach used to

390 obtain the 1 km soil moisture maps, in which the lack of Land Surface Temperature (LST)

391 information from MODIS visible/infrared (VIS/IR) satellite data in cloudy conditions (section

392 2.2) constrains derived-SSM information. The availability and usefulness of this product is

393 therefore significantly reduced. The new product L4$^{3.0}$, used in this study, in which the

394 previous limitation is resolved using ERA-Interim-derived LST information, shows a

395 coverage percentage in the order of 92 %, even higher than the SMOS-L3 and -L2 products.

396 However, Figure 2b demonstrates that the spatial representation of the seasonal mean does not

397 improve with this product, as a consequence of the limited temporal availability of the

398 SMOS-derived SSM product dictated by the revisit period of the satellite.

399 In Figure 3, only common available days from all different operational levels are selected for

400 an inter-SMOS product comparison. When remapped to the same resolution (coarser grid

401 spacing) comparable values are identified between SMOS-L3, -L2 and –L4$^{3.0}$ for the JJA and

402 SON period, whereas relevant differences are pointed out from December to May. In this last

403 period, we identify higher means for the SMOS-L4$^{3.0}$ product and SMOS-L3 with respect to

404 SMOS-L2, which is in agreement with a systematic dry bias identified for SMOS-L2 also in

405 previous studies (section 1).

406 At sub-seasonal scales, e.g. event scale on the 19-20 November 2012 (Figure 4), the SMOS-

407 L4$^{\mathbf{3.0}}$ product shows SSM mean and variability in the same range of the SMOS-L2 and -L3

408 products, but with a finer-improved resolution representation of the spatial distribution.

409 Comparisons with the mean ground-based SSM at the VAS (OBS area: *0.25 ±0.0002*) show

410 better agreement with the mean SSM from the SMOS-L4$^{3.0}$-1 km disaggregated product

411 (*0.23±0.002*) and poorer correlation with SMOS-L2 (*0.20±0.002*). The problematic of SMOS-

412 L4$^{3.0}$ on seasonal time scales vanishes at sub-seasonal (event) scales where the potential

413 added value of the 1 km product is manifest.

414 4.1.2 Temporal evolution of surface soil moisture data sets

The SMOS and in situ measured SSM time series are investigated and compared in this section in Figures 5 and 6 over the IP, the VAS (50x50 km2) and the OBS (10x10 km2) areas. Overall, the averaged SMOS-L2 and -L4$^{3.0}$ data over the IP are much more variable than the SMOS-L3, showing a more extreme daily index (SMOS-L2: -1 to 2; SMOS-L4$^{3.0}$: -0.7 to 1.45). Over the VAS, SMOS-L2 is clearly more variable than the higher resolution SMOS-L4$^{3.0}$. But, the last one shows a wider range of values as well as more extreme daily index values when compared to the averaged in situ soil moisture measurements. The CVs of the spatially averaged SMOS-L4$^{3.0}$ is lower than those of SMOS-L3, -L2 and in situ observations indicating that this data are less scattered. Despite detected differences within in situ observations, SMOS responds well to soil moisture variations over time.

Although absolute values are not totally captured, all three SMOS products adequately reproduce the temporal dynamics at a regional scale. The systematic dry bias present on SMOS-L2 data (Piles et al. 2014) is evident particularly on the first half of the year. A mean bias in the order of -0.09 to -0.07 m^3/m^3 is identified for the DJF-MAM period; this difference is reduced to -0.02 m^3/m^3 for the JJA-SON period (Table 3). During the DJF-MAM period the vineyards are bare, only the vine stocks are present. The water content of the vine stocks negatively impacts the SMOS measurements (Schwank et al. 2012).

Good agreement is found between the SMOS-L4$^{3.0}$ product and the mean of the in situ observations (the network's variability (shaded grey) contains the SMOS-L4$^{3.0}$ data). Scores confirm this result particularly for the periods DJF and SON (slope~1, R^2~0.7). Poorer correlation is found for the MAM (slope~0.6, R^2~0.4). In this period, soil moisture maxima immediately after the precipitation events are not always well captured by the SMOS-L4$^{3.0}$ data, showing additionally a too rapid drying after this. This observation agrees with the SMOS' inability of correctly measuring in situations when liquid water is present at the soil. The measured signal is perturbed during the vegetation growing season, which could explain

440   the worse statistics. On the other hand, during JJA, low slope~0.1 and R^2~0.01 could be in

441   relation to SSM values close to or lower than 0.1 m^3/m^3 and very low spatial variability,

442   which was found to be necessary for an adequate performance of the algorithm used for the

443   derivation of the SMOS-L4 1 km product in Molero et al. (2016).

444   4.2 Spatial comparison at high-resolution: SMOS-L4$^{3.0}$ versus ground measurements

445   High-resolution spatio-temporal correlations are assessed by spatial comparison with in situ

446   observations. Characteristics of each of the in-situ stations are presented in Table 1. A

447   seasonal analysis is performed focusing on the selected year of measurements covering a

448   complete hydrological cycle (from 1 December 2011 to 31 December 2012). Comparisons

449   between SMOS-L2 and ground measurements are additionally included. Statistics for

450   individual comparisons at all stations are summarized in Table 3. Comparisons between

451   SMOS-L3 and ground measurements were similarly performed evidencing the expected bad

452   correlations (R^2 ~ 0,002, not shown)In Figure 7, the scatter plots display (a) possible

453   differences between dry and wet days (> 1 mm/d), and (b, c) the agreement between remotely

454   sensed and in situ soil moisture measurements from the OBS network using the seasonal

455   classification. To consider any uncertainties arising from spatial averaging, ground

456   measurements are compared to point like and 10x10 km^2 SSM means. The 10x10 km^2 area

457   used covers the OBS area, i.e., the network of in situ measurements within the VAS. For

458   comparison, all grid points from SMOS-L4$^{3.0}$ and SMOS-L2 included within the area are

459   considered.

460   In Figure 7a, the separation between days with and without precipitation (< 1 mm/d) points

461   out similar correlations during dry than wet days (RMSD~0.015, R^2~0.7) for SMOS-L4$^{3.0}$,

462   whereas a slightly better agreement is found for the dry days (not shown) for SMOS-L2. A

463   systematic mean dry bias of about 0.05 (dry days) to 0.08 (wet days) m^3/m^3 is assessed for

464   SMOS-L2, while a lower bias with changing sign is identified for the L4$^{3.0}$ product (~ 0.005

465 (wet days); ~ -0.02 (dry days)). Comparisons using the corresponding mean over the 10x10

466 km^2 OBS area, in Figure 7b and Table 3, show good agreement with respect to the SMOS-

467 L4$^{3.0}$ and poorer scores for SMOS-L2 (only one grid point of SMOS-L2 is located within the

468 OBS area). Worse consistency is found in both cases for the MAM and JJA periods. CRMSD

469 is in all cases in the required range of ≤ 0.04 m^3/m^3. Point-like comparisons with the

470 individual in situ stations, in Figure 7c and Table 3, show that spatial patterns are captured at

471 1km with RMSD~0.007 to 0.1 m^3/m^3 but, in most cases, accuracy for SMOS-L4$^{3.0}$-1 km

472 disaggregated product is within the required range of less than 0.04 m^3/m^3 (not shown).

473 Higher RMSD is found for SMOS-L2, ~ 0.008 to 0.13 m^3/m^3, accounting for the previously

474 identified dry bias (~ (-0.14) − (-0.02)) reduced in SMOS-L4$^{3.0}$ (~ (-0.08) − (-0.01)). The

475 CRMSD is in all cases ≤ 0.04 m^3/m^3. For all stations, better correlations are found in DJF and

476 SON and poorer scores in JJA and MAM, in agreement with the areal-mean comparisons

477 (section 4.1.3). Best scores are obtained for Nicolas, VAS and La Cubera stations, probably in

478 relation to their common soil type distribution, over vineyards, and homogeneous conditions,

479 over a plain (Figure 8a, Table 3). The SON time period reveals the best agreement, at this

480 time the vineyards are completely grown (however, senescent thus containing less water) and

481 SSM exhibits substantial spatial variability driven by precipitation and irrigation thus

482 improving spatio-temporal correlations. Worse statistics are found for Melbex-I, Melbex-II

483 and Ezpeleta, probably in relation to the location of the soil moisture probes in rockier and

484 orographically more complex areas, also in proximity to forestall and man-made construction

485 areas.

486 The soil moisture probability distribution function (PDF; Figure 8b) of all in situ

487 measurements versus SMOS-L4$^{3.0}$ data reveals that the later overestimates SSM below 0.1

488 m^3/m^3, values mainly observed during the JJA period. But, an underestimation occurs in the

489 range between 0.1 and 0.3 m^3/m^3, which is consistent with the identified underestimation of

490   maximum soil moisture reached after a precipitation event and the rapid drying of the soil in

491   comparison to the much slower response seen in the observations during the MAM period

492   (Figure 6c).

493   4.3 SURFEX model simulations and realistic initialization with 1-km soil moisture data

494   4.3.1 SURFEX model simulations of selected stations and realistic initialization

495   As a first step, the performance of the SURFEX(ISBA) SVAT model is evaluated.

496   SURFEX(ISBA) point-like simulations are performed for all in situ soil moisture stations at

497   the VAS area to assess the usefulness of the model for further investigation (Table 4).

498   SURFEX(ISBA) simulations show good agreement with soil moisture ground-based

499   observations at all stations, adequately capturing the associated spatio-temporal variability

500   (slope~1, R^2~ 0.7 to 0.9; MB~0.1 m^3/m^3; CRMSD~0.02 m^3/m^3). It can be concluded that the

501   model performs well and is therefore suitable for further investigation. The seasonal analysis

502   points out the best simulations in the SON period (R^2~0.9 for all stations), but CRMSD is $\leq$

503   0.04 m^3/m^3 for all stations at all periods.

504   Using the mean of the ground-based measurement on the day of the model simulation

505   initialization (realistic initialization; REAL-I) the temporal mean comparison for each station

506   presented in Figure 9 and Table 4 reveals mean R^2~0.8 when the all hydrological year is

507   considered.

508   4.3.2 Spatialization

509   As a first step, point-scale SURFEX-ECMWF and SURFEX-SAFRAN simulations covering

510   the whole investigation period are performed for all in situ soil moisture stations to examine

511   its ability to reproduce soil moisture dynamics. Ground measurements at each station are used

512   for initialization. Scores clearly indicate better agreement with all in situ observations for the

22

513　SURFEX-SAFRAN simulations (slopes~ 1, R^2~ 0.9, RMSD< 0.1 m^3/m^3), rather than the

514　SURFEX-ECMWF simulations (slopes> 1, R^2~ 0.6, and RMSD> 0.1 m^3/m^3).

515　In a second step, SURFEX-ECMWF and SURFEX-SAFRAN simulations are spatialized to

516　obtain maps of soil moisture over the investigation area. In our CTRL simulations, the daily

517　soil moisture from the mean of the in-situ measurements on the initialization day is used for

518　model initialization. Mean SSM from in situ measurements for the whole investigation period

519　is in the order of 0.14±0.005, whereas SURFEX-ECMWF derived SSM field is about

520　0.18±0.007 and SURFEX-SAFRAN derived SSM field is 0.15±0.002, thus, closer to ground-

521　based observations. Performing a seasonal analysis, we demonstrate that this consistency is

522　maintained for all seasons (not shown). The higher resolution of the SAFRAN-atmospheric

523　forcing better reproduces the high spatial heterogeneity over the VAS area resulting in

524　improved mapping of simulated SSM.

525　To exemplify the importance and implications of soil moisture initialization several

526　experiments are performed. Initialization of the SURFEX-SAFRAN simulation using SMOS-

527　$L4^{3.0}$ (EXP-SMOS) is examined against a sensitivity simulation using for the initial soil

528　moisture scenario the climatological soil moisture from observations (daily mean over 10

529　years, which has been selected to be far from observations; EXP-CLIM). These experiments

530　are initialized in dry periods, following Khodayar et al. (2014) recommendations, to

531　maximize the impact, and run for about 3-4 months. In the first case, initialization is

532　performed in a winter month (December) and the whole simulation period remains almost

533　dry. In the second case, a summer month (July) is chosen for the initialization and it is

534　followed by a wet autumn period with frequent heavy precipitation events in the area.

535　The temporal evolution of the RMSD (Figure 10a) demonstrates that the initial soil moisture

536　scenario influences its evolution until the end of the simulation, in agreement with previous

537　results in section 4.3.1. Larger deviations occur during dry periods, in both scenarios. Longer

23

538   spin-up times, defined as the time that soil needs to re-establish quasi-equilibrium,

539   characterize the dry scenario. It is after heavy precipitation events that deviations decrease.

540   Soil quickly reacts to changes in the precipitation field in the semi-arid IP. When the upper

541   level soil gets close to saturation soil memory is almost lost. Before the high precipitation

542   events, SSM evolves following the direction of the initial perturbation, i.e., higher initial SSM

543   yields higher SSM, however, a stochastic behaviour is identified afterwards.

544   As an example, differences in the spatial distribution of soil moisture for the winter/dry period

545   simulation are discussed (Figure 10b). A relevant difference in the mean is identified when

546   compared to the CTRL simulation (0.17±0.004): EXP-CLIM (0.014±0.003), EXP_SMOS

547   (0.17±0.003). Clearly, better agreement is found in this last case.

548   Considering the EXP-SMOS initialization scenario simulation, a comparison between

549   simulated point-like and the 10x10 km^2 mean against corresponding ground measurements

550   was done for verification (Figure 10c). Correlations in the order of R^2~0.9 confirm that the

551   combined use of SURFEX-SAFRAN and SMOS-L4$^{3.0}$ for initialization successfully

552   reproduces soil moisture spatial and temporal variability becoming an optimal tool for

553   mapping soil moisture heterogeneity over a study region for diverse purposes.

554

555   **5. Discussion and conclusions**

556   High-resolution soil moisture products are essential for our understanding of hydrological and

557   climatic processes as well as improvement of model skills. Due to its high spatial and

558   temporal variability, it is a complicated variable to assess. Mapping high-resolution soil

559   moisture fields using intensively collected in-situ measurements is infeasible. Thus, state of

560   the art high-resolution modelling and satellite-derived products have to fill this gap, although

561   verification is needed. In this study, we examine the potential of the state of the art SMOS-

562 L4$^{3.0}$-1 km "all weather" disaggregated product for assessment of soil moisture variability,

563 and improvement of the SVAT SURFEX(ISBA) simulations, in combination with the

564 SAFRAN meteorological analysis system (SURFEX-SAFRAN), through realistic

565 initialization. A dense network of ground-based soil moisture measurements over the

566 Valencia Anchor Station (VAS; one of the SMOS test sites in Europe) is used for verification.

567 The proposed analysis focuses on the semi-arid IP and covers the one year period of 2012

568 (from December 2011 to December 2012). The comparison of the SMOS-L4$^{3.0}$-1km product

569 to different grid spacing soil moisture data products from SMOS, namely SMOS-L3 (~ 25

570 km) and SMOS-L2 (~15 km) shows that on seasonal time scales SMOS-L4$^{3.0}$ does not

571 accurately capture the spatial variability of the soil moisture field, contrary to SMOS-L3 and

572 SMOS-L2, despite the novelty of introducing ERA-Interim LST data in the MODIS

573 LST/NDVI space (Piles et al. 2014; Sanchez-Ruiz et al. 2014). This is probably in relation to

574 the so different spatial resolution of ERA-Interim and MODIS. This new downscaling

575 approach greatly enhances the potential applicability of the data for those days/periods in

576 which measurements are available, but cannot accurately fill in those periods without

577 measurements dictated by the revisit period of the SMOS satellite, hence, compromising the

578 soil moisture representation as a mean for longer periods than a day. On sub-seasonal time

579 scales, when SMOS images are available, the SMOS-L4$^{3.0}$ high-resolution product shows its

580 potential. It adequately captures the surface soil moisture variability in association with the

581 precipitation field, also when extreme precipitation takes place.

582 Mean and single station comparisons with in-situ measurements reveal that characteristics of

583 SMOS-L4$^{3.0}$ soil moisture fields are closer to in-situ observations than SMOS-L3 and -L2

584 products. Point-like and 10x10 km^2 comparisons show good agreement with respect to the

585 SMOS-L4$^{3.0}$ and poorer scores for SMOS-L2 (e.g. DJF period: SMOS-L3/-L2: Slope:1.1/1.0,

586 R^2:0.5/0.7, Bias:-0.09/(-0.03)). Generally, all three SMOS products adequately reproduce the

587 soil moisture temporal dynamics meeting the desired accuracy of the mission (0.04 m3/m3);

588 however, the spatial patterns did not always reach the expected precision in agreement with

589 former studies in other regions (Gonzalez-Zamora et al. 2015). Comparisons with ground soil

590 moisture measurements from the eight stations in the OBS network (10x10 km^2) over the

591 VAS area shows that the spatial patterns are captured at 1 km with RMSD~ 0.007 to 0.1

592 m^3/m^3. The best correlations are in DJF and SON, and poorer scores in MAM and JJA, in

593 agreement with the areal-mean comparisons. SMOS-L4$^{3.0}$ data shows better agreement at

594 those stations over plain areas and with uniform conditions (vineyards), against those over

595 more complex and less homogeneous terrains (rocky soils and areas close to forestall and

596 man-made constructions). The SMOS-L4$^{3.0}$ soil moisture probability distribution function

597 (PDF) in comparison to that of the in-situ measurements reveals a SMOS overestimation

598 below 0.1 m^3/m^3 and an underestimation in the range between 0.1 to 0.3 m^3/m^3. A seasonal

599 analysis points out better scores for the DJF and SON periods, whereas poorer correlation is

600 found for the MAM and JJA periods. In the MAM period, an under-representation of the

601 rainy events is found, as well as faster and stronger drying changes coinciding with the

602 vegetation growth season. In JJA, the very low soil moisture values (< 0.1 m^3/m^3) with

603 associated low spatial variability results in low R^2. No significant differences are found during

604 dry and wet days (> 0.1 mm/d).

605 SURFEX(ISBA) SVAT simulations covering the whole investigation period over all in-situ

606 measurement stations at the VAS area show good agreement with ground-based observations.

607 Mean values are well reproduced for all stations and the temporal variability is well captured

608 (R2~0.7 to 0.95; RMSD~0.02). The synergetic use of SURFEX(ISBA) simulations with

609 SAFRAN atmospheric forcing information initialized with realistic SSM values from the

610 SMOS-L4$^{3.0}$ data set was successful combination to obtain soil moisture maps over the VAS

611 domain. Good agreement was reached when comparisons between point-like and 10x10 km^2

612   simulations with SURFEX-SAFRAN initialized with SMOS-L4$^{3.0}$ data and in-situ soil

613   moisture measurements were made (R^2~0.9 and RMSD<0.04 m^3/m^3).

614   In this study, the comparison and suitability of different operational satellite products from the

615   SMOS platform is investigated to provide realistic information on the water content of the

616   soil. The comparison carried out helps drawing guidelines on best practices for the sensible

617   use of these products. Currently, there is not a consensus about what is the "best" SMOS

618   product. Different users utilize different products depending on their application rather than

619   based on performance arguments. This study and the conclusions obtained on the comparison

620   are important to provide information on the advantages and drawbacks of these datasets. The

621   high temporal and spatial resolution soil moisture maps obtained in this study could be of use

622   for hydrological and agronomical applications, to build climatologies of SSM, as initial

623   condition for convective system modelling, for flood forecasting and for downstream local

624   applications such as crop monitoring and crop development strategies as well as for irrigation

625   data sets, among others. Additionally, an accurate representation of SSM will permit the

626   calculation of SM profiles by application of e.g. exponential filters, which has been

627   demonstrated to be a successful technique. Furthermore, the added value of the SMOS-L4$^{3.0}$-1

628   km disaggregated product for initialization purposes is demonstrated, which suggests its

629   potential for assimilation purposes. These two last aspects are out of the scope of this paper,

630   but they are investigated in detail in a follow-up study. Important aspects of the SMOS-L4$^{3.0}$

631   SSM product have still to be improved, namely its temporal availability (e.g. successful

632   investigations on the increase of SMOS-L3 temporal resolution to 3h are available (Louvet et

633   al. 2015)), its spatio-temporal correlation with in situ measurements over complex

634   topographic areas, in areas/periods with low spatial variability and in rainy periods when an

635   under-representation and rapid decay of SSM has been identified.This study also points out

636   that in order to more accurately examine the reproducibility of the high spatial variability of

637 this variable by the newly available satellite derived downscaled high-resolution soil moisture

638 observations, large and dense networks of in situ soil moisture measurements covering

639 different soil types and land uses as well as considering different soil depths are needed. In an

640 effort to come a step forward in this direction, dedicated long-term networks with the

641 previously described characteristics should be established permanently in different regions

642 around the world.

643

644

658

659

660

661

References

663 ARRAY Systems Computing Inc., CESBIO, IPSL-Service d'Aéronomie, INRA-EPHYSE,
664 Reading University, Tor Vergata University. Algorithm Theoretical Basis Document (ATBD)
665 for the SMOS Level 2 Soil Moisture Processor Development Continuation Project. ESA No.:
666 SO-TN-ARR-L2PP-0037 Issue: 3.9 Array No.: ASC_SMPPD_037 Date: October 24, 2014

667

668 Bircher, S., Skou, N., Jensen, K. H., Walker, J. P., & Rasmussen, L. (2012). A soil moisture
669 and temperature network for SMOS validation in Western Denmark. Hydrology and Earth
670 System Sciences, 16(5), 1445-1463.

671

672 Bolle, H.-J., Eckardt, M., Koslowsky, D., Maselli, F., Meliá Miralles, J., Menenti, M., Olesen,
673 F.-S., Petkov, L., Rasool, I., Van de Griend, A.A. (Editors). Contributing Authors: H. Billing,
674 A. Gitelson, F. Göttsche, A. Jochum-Osann, E. Lopez-Baeza, F. Meneguzzo, J. Moreno, F.
675 Nerry, P. Rossini, F. Veroustraete, R. Vogt, P.J. Van Oeleven. Mediterranean Landsurface
676 Processes Assessed From Space. Chapter 6 From Research to Application. Regional Climate
677 Studies Series. Springer-Verlag Berlin Heidelberg, ISBN: 978-3-540-40151-3 (Print) 978-3-
678 540-45310-9 (Online) (2006)

679

680 Boone, A., Calvet, J.-C., & Noilhan, J. (1999). Inclusion of a Third Soil Layer in a Land
681 Surface Scheme Using the Force–Restore Method. Journal of Applied Meteorology, 38,

682 1611–1630. https://doi.org/10.1175/1520-0450(1999)038<1611:IOATSL>2.0.CO;2

683 Bosch, D. D., J. M. Sheridan, and L. K. Marshall (2007), Precipitation, soil moisture, and

684 climate database, Little River Experimental Watershed, Georgia, United States, Water Resour.

685 Res., 43, W09472, doi:10.1029/2006WR005834

686

687 Brocca, L., Melone, F., Moramarco, T., Wagner, W., & Hasenauer, S. (2010). ASCAT soil

688 wetness index validation through in situ and modeled soil moisture data in central Italy.

689 Remote Sensing of Environment, 114(11), 2745-2755.

690

691 Calvet, J.-C., Noilhan, J., & Bessemoulin, P. (1998). Retrieving the Root-Zone Soil Moisture

692 from Surface Soil Moisture or Temperature Estimates: A Feasibility Study Based on Field

693 Measurements.   Journal   of   Applied   Meteorology,   37(1995),   371–386.

694 https://doi.org/10.1175/1520-0450(1998)037<0371:RTRZSM>2.0.CO;2

695

696 Clapp, R. B., & Hornberger, G. M. (1978). Empirical equations for some soil hydraulic

697 properties. Water resources research, 14(4), 601-604.

698

699 Cosby, B. J., Hornberger, G. M., Clapp, R. B., & Ginn, T. (1984). A statistical exploration of

700 the relationships of soil moisture characteristics to the physical properties of soils. Water

701 resources research, 20(6), 682-690.

702

703   Cosh, M. H., Jackson, T. J., Bindlish, R., & Prueger, J. H. (2004). Watershed scale temporal

704   and spatial stability of soil moisture and its role in validating satellite estimates. Remote

705   sensing of Environment, 92(4), 427-435.

706

707   Djamai, N., Magagi, R., Goïta, K., Merlin, O., Kerr, Y., Roy, A. (2016). A combination of

708   DISPATCH downscaling algorithm with CLASS land surface scheme for soil moisture

709   estimation at fine scale during cloudy days. Remote Sensing of Environment, 184, 1-14.

710

711   De Lannoy, G. J., & Reichle, R. H. (2016). Global assimilation of multiangle and

712   multipolarization SMOS brightness temperature observations into the GEOS-5 catchment

713   land surface model for soil moisture estimation. Journal of Hydrometeorology, 17(2), 669-

714   691.

715

716   Delwart, S., Bouzinac, C., Wursteisen, P., Berger, M., Drinkwater, M., Martín-Neira, M., &

717   Kerr, Y. H. (2008). SMOS validation and the COSMOS campaigns. IEEE Transactions on

718   Geoscience and Remote Sensing, 46(3), 695-704.

719

720   Dente, L., Su, Z., & Wen, J. (2012). Validation of SMOS soil moisture products over the

721   Maqu and Twente regions. Sensors, 12(8), 9965-9986.

722

723   Drobinski P., V. Ducrocq, P. Alpert, E. Anagnostou, K. Béranger, M. Borga, I. Braud, A.

724   Chanzy, S. Davolio, G. Delrieu, C. Estournel, N. Filali Boubrahmi, J. Font, V. Grubišić, S.

725   Gualdi, V. Homar, B. Ivančan-Picek, C. Kottmeier, V. Kotroni, K. Lagouvardos, P. Lionello,

726   M. C. Llasat, W. Ludwig, C. Lutoff, A. Mariotti, E. Richard, R. Romero, R. Rotunno, O.

727   Roussot, I. Ruin, S. Somot, I. Taupier-Letage, J. Tintore, R. Uijlenhoet, and H. Wernli, 2014.

728   HyMeX: A 10-year multidisciplinary program on the Mediterranean water cycle. Bull. Amer.

729   Meteor. Soc., 95, 1063–1082. doi: http://dx.doi.org/10.1175/BAMS-D-12-00242.1

730

731   Ducrocq Véronique, Isabelle Braud, Silvio Davolio, Rossella Ferretti, Cyrille Flamant,

732   Agustin Jansa, Norbert Kalthoff, Evelyne Richard, Isabelle Taupier-Letage, Pierre-Alain

733   Ayral, Sophie Belamari, Alexis Berne, Marco Borga, Brice Boudevillain, Olivier Bock, Jean-

734   Luc Boichard, Marie-Noëlle Bouin, Olivier Bousquet, Christophe Bouvier, Jacopo Chiggiato,

735   Domenico Cimini, Ulrich Corsmeier, Laurent Coppola, Philippe Cocquerez, Eric Defer,

736   Julien Delanoë, Paolo Di Girolamo, Alexis Doerenbecher, Philippe Drobinski, Yann

737   Dufournet, Nadia Fourrié, Jonathan J. Gourley, Laurent Labatut, Dominique Lambert, Jérôme

738   Le Coz, Frank S. Marzano, Gilles Molinié, Andrea Montani, Guillaume Nord, Mathieu Nuret,

739   Karim Ramage, William Rison, Odile Roussot, Frédérique Said, Alfons Schwarzenboeck,

740   Pierre Testor, Joël Van Baelen, Béatrice Vincendon, Montserrat Aran, and Jorge Tamayo,

741   2014. HyMeX-SOP1: The field campaign dedicated to heavy precipitation and flash flooding

742   in the Northwestern Mediterranean. Bull. Amer. Meteor. Soc., 95, 1083–1100. doi:

743   http://dx.doi.org/10.1175/BAMS-D-12-00244.1

744

745   Duffourg, F., & Ducrocq, V. (2011). Origin of the moisture feeding the Heavy Precipitating

746   Systems over Southeastern France. Natural Hazards and Earth System Sciences, 11(4), 1163.

747

748 Duffourg, F., & Ducrocq, V. (2013). Assessment of the water supply to Mediterranean heavy

749 precipitation: a method based on finely designed water budgets. Atmospheric Science Letters,

750 14(3), 133-138.

751

752 Durand, Y., E. Brun, L. Mérindol, G. Guyomarc'h, B. Lesaffre, E. Martin, A meteorological

753 estimation of relevant parameters for snow models, Ann. Glaciol. 18 (1993) 65–71.

754

755 Durand, Y., G. Giraud, M. Laternser, P. Etchevers, L. Mérindol, B. Lesaffre, Reanalysis of 47

756 Years of Climate in the French Alps (1958–2005): Climatology and Trends for Snow Cover,

757 J. Appl. Meteorol. Climatol. 48 (2009) 2487–2512.

758

759 Entekhabi, D., Rodriguez-Iturbe, I., & Castelli, F. (1996). Mutual interaction of soil moisture

760 state and atmospheric processes. Journal of Hydrology, 184(1-2), 3-17.

761

762 Entekhabi, D.; Njoku, E.G.; Neill, P.E.; Kellogg, K.H.; Crow, W.T.; Edelstein,W.N.; Entin,

763 J.K.; Goodman, S.D.; Jackson, T.J.; Johnson, J. The soil moisture active passive (SMAP)

764 mission (2010). Proc. IEEE, 98, 704–716.

765

766 FAO; World reference base for soil resources 2014 international soil classification system for

767 naming soils and creating legends for soil maps. Rome: FAO, 2014.

768

769   Gherboudj, I., Magagi, R., Goïta, K., Berg, A. A., Toth, B., & Walker, A. (2012). Validation

770   of SMOS data over agricultural and boreal forest areas in Canada. IEEE Transactions on

771   Geoscience and Remote Sensing, 50(5), 1623-1635.

772

773   GTOPO30 Documentation, U.S. Geological Survey, 1996, Global 30 Arc-Second Elevation

774   A. Gonzalez-Zamora, N. Sánchez, J. Martinez-Fernandez, A. Gumuzzio, M. Piles, E.

775   Olmedo. Long-Term SMOS Soil Moisture Products: A Comprehensive Evaluation across

776   Scales and Methods in the Duero Basin Physics and Chemistry of the Earth, Parts A/B/C, 83–

777   84 (2015), pp. 123–136 http://dx.doi.org/10.1016/j.pce.2015.05.009

778

779   Hirschi, M., Seneviratne, S. I., Alexandrov, V., Boberg, F., Boroneant, C., Christensen, O. B.,

780   and Stepanek, P. (2011). Observational evidence for soil-moisture impact on hot extremes in

781   southeastern Europe. Nature Geoscience, 4(1), 17.

782

783   Jansa, J., Erb, A., Oberholzer, H. R., Šmilauer, P., & Egli, S. (2014). Soil and geography are

784   more important determinants of indigenous arbuscular mycorrhizal communities than

785   management practices in Swiss agricultural soils. Molecular ecology, 23(8), 2118-2135.

786

787   Jones, M. O., L. A. Jones, J. S. Kimball, and K. C. McDonald (2011), Satellite passive

788   microwave remote sensing for monitoring global land surface phenology, Remote Sens.

789   Environ., 115(4), 1102–1114, doi:10.1016/j.rse.2010.12.015.

790

791 Juglea, S., Kerr, Y., Mialon, A., Lopez-Baeza, E., Braithwaite, D., & Hsu, K. (2010). Soil

792 moisture modelling of a SMOS pixel: Interest of using the PERSIANN database over the

793 Valencia Anchor Station. Hydrology and Earth System Sciences, 14(8), 1509–1525.

794 https://doi.org/10.5194/hess-14-1509-2010

795

796 Juglea, S., Kerr, Y., Mialon, A., Wigneron, J. P., Lopez-Baeza, E., Cano, A., … Delwart, S.

797 (2010). Modelling soil moisture at SMOS scale by use of a SVAT model over the Valencia

798 Anchor Station. Hydrology and Earth System Sciences, 14(5), 831–846.

799 https://doi.org/10.5194/hess-14-831-2010

800

801 Kerr, Y. H. (2007). Soil moisture from space: Where are we?. Hydrogeology journal, 15(1),

802 117-120.

803

804 Kerr, Y. H., Waldteufel, P., Wigneron, J. P., Delwart, S., Cabot, F., Boutin, J., ... & Juglea, S.

805 E. (2010). The SMOS mission: New tool for monitoring key elements ofthe global water

806 cycle. Proceedings of the IEEE, 98(5), 666-687.

807

808 Kerr, Y. H., Waldteufel, P., Wigneron, J. P., Martinuzzi, J. A. M. J., Font, J., & Berger, M.

809 (2001). Soil moisture retrieval from space: The Soil Moisture and Ocean Salinity (SMOS)

810 mission. IEEE transactions on Geoscience and remote sensing, 39(8), 1729-1735.

811

812   Khodayar, S., Raff, F., Kalthoff, N. 2015. Dignostic Study of a High Precipitation Event   in

813   the Western Mediterranean Region: Adequacy of Current operational Networks

814   Quart. J. Roy. Meteor. Soc. DOI: 10.1002/qj.2600

815

816   Khodayar, S., Sehlinger, A., Feldmann, H., & Kottmeier, C. (2015). Sensitivity of soil

817   moisture initialization for decadal predictions under different regional climatic conditions in

818   Europe. International Journal of Climatology, 35(8), 1899-1915.

819

820   Koster, R. D., Dirmeyer, P. A., Guo, Z., Bonan, G., Chan, E., Cox, P., ... & Liu, P. (2004).

821   Regions of strong coupling between soil moisture and precipitation. Science, 305(5687),

822   1138-1140.

823

824   Le Moigne, P., Boone, A., Calvet, J. C., Decharme, B., Faroux, S., Gibelin, A. L., ... &

825   Mironov, D. (2009). SURFEX scientific documentation. Note de centre (CNRM/GMME),

826   Météo-France, Toulouse, France.

827

828   Liu, Y.Y.; Parinussa, R.M.; Dorigo, W.A.; De Jeu, R.A.M.; Wagner, W.; van Dijk, A.I.J.M.;

829   McCabe, M.F.; Evans, J.P. Developing an improved soil moisture dataset by blending passive

830   and active microwave satellite-based retrievals (2011). Hydrol. Earth Syst. Sci., 15, 425–436.

831

832   Louvet, S., Thierry Pellarin, Ahmad al Bitar, Bernard Cappelaere, Sylvie Galle, Manuela

833   Grippa, Claire Gruhier, Yann Kerr, Thierry Lebel, Arnaud Mialon, Eric Mougin, Guillaume

834   Quantin, Philippe Richaume, Patricia de Rosnay (2015). SMOS soil moisture product

835   evaluation over West-Africa from local to regional scale. Remote Sensing of Environment,

836   Volume 156, Pages 383-394, ISSN 0034-4257, DOI: 10.1016/j.rse.2014.10.005.

837

838   Malbéteau, Y., Merlin, O., Balsamo, G., Er-Raki, S., Khabba, S.,Walker, J. P., Jarlan, L.

839   (2018). Toward a Surface Soil Moisture Product at High Spatiotemporal Resolution:

840   Temporally Interpolated, Spatially Disaggregated SMOS Data. Journal of Hydrometeorology,

841   19(1), 183-200.

842

843   Masson, V., Champeaux, J. L., Chauvin, F., Meriguet, C., & Lacaze, R. (2003). A global

844   database of land surface parameters at 1-km resolution in meteorological and climate models.

845   Journal of Climate, 16(9), 1261–1282. https://doi.org/10.1175/1520-0442-16.9.1261

846

847   Merlin, O., Rüdiger, C., Al Bitar, A., Richaume, P., Walker, J. P., & Kerr, Y. H. (2012).

848   Disaggregation of SMOS soil moisture in Southeastern Australia. IEEE Transactions on

849   Geoscience and Remote Sensing, 50(5), 1556–1571. http://dx.doi.org/10.1109/TGRS.

850   2011.2175000.

851   Naeimi, V.; Scipal, K.; Bartalis, Z.; Hasenauer, S.; Wagner, W. An improved soil moisture

852   retrieval algorithm for ers and metop scatterometer observations (2009). IEEE Trans. Geosci.

853   Remote Sens. 47, 1999–2013.

854

855   Noilhan, J., & Planton, S. (1989). A Simple Parameterization of Land Surface Processes for

856   Meteorological Models. Monthly Weather Review. https://doi.org/10.1175/1520-

857   0493(1989)117<0536:ASPOLS>2.0.CO;2

858   Owe, M.; de Jeu, R.; Holmes, T. Multisensor historical climatology of satellite-derived global

859   land surface moisture (2008). J. Geophys. Res. Earth Surf., 113, F01002.

860

861   Piles, M., Camps, A., Vall-Llossera, M., Corbella, I., Panciera, R., Rudiger, C., … Walker, J.

862   (2011). Downscaling SMOS-derived soil moisture using MODIS visible/infrared data. IEEE

863   Transactions   on   Geoscience   and   Remote   Sensing,   49(9),   3156–3166.

864   https://doi.org/10.1109/TGRS.2011.2120615

865

866   Piles, M., Sánchez, N., Vall-Llossera, M., Camps, A., Martínez-Fernandez, J., Martinez, J., &

867   Gonzalez-Gambau, V. (2014). A downscaling approach for SMOS land observations:

868   Evaluation of high-resolution soil moisture maps over the Iberian peninsula. IEEE Journal of

869   Selected Topics in Applied Earth Observations and Remote Sensing, 7(9), 3845–3857.

870   https://doi.org/10.1109/JSTARS.2014.2325398

871

872   Piles, M., Vall-Llossera, M., Camps, A., Sanchez, N., Martinez-Fernandez, J., Martinez, J., …

873   Riera, R. (2013). On the synergy of SMOS and Terra/Aqua MODIS: High resolution soil

874   moisture maps in near real-time. International Geoscience and Remote Sensing Symposium

875   (IGARSS), 3423–3426. https://doi.org/10.1109/IGARSS.2013.6723564

876

877   Piles, M., Pou, X., Camps, A., Vall-llosera, M. (2015): Quality report: Validation of SMOS-

878   BEC L4 high resolution soil moisture products, version 3.0 or "all-weather". Technical report.

879   Available at: http://bec.icm.csic.es/doc/BEC-SMOS-L4SMv3-QR.pdf

880

881 Quintana-Segui, P., Le Moigne, P., Durand, Y., Martin, E., Habets, F., Baillon, M., ... &

882 Morel, S. (2008). Analysis of near-surface atmospheric variables: Validation of the SAFRAN

883 analysis over France. Journal of applied meteorology and climatology, 47(1), 92-107.

884

885 Quintana-Seguí, P., Peral, C., Turco, M., Llasat, M. C., & Martin, E. (2016). Meteorological

886 Analysis Systems in North-East Spain: Validation of SAFRAN and SPAN. Journal of

887 Environmental Informatics, 27(2).

888

889 Raveh-Rubin, S., and Wernli, H. (2015). Large-scale wind and precipitation extremes in the

890 Mediterranean: a climatological analysis for 1979–2012. Quarterly Journal of the Royal

891 Meteorological Society, 141(691), 2404-2417.

892

893 Robock, A., Vinnikov, K. Y., Srinivasan, G., Entin, J. K., Hollinger, S. E., Speranskaya, N.

894 A., ... & Namkhai, A. (2000). The global soil moisture data bank. Bulletin of the American

895 Meteorological Society, 81(6), 1281-1299.

896

897 Rosenbaum, U., H. R. Bogena, M. Herbst, J. A. Huisman, T. J. Peterson, A. Weuthen, A. W.

898 Western, and H. Vereecken (2012), Seasonal and event dynamics of spatial soil moisture

899 patterns   at   the   small   catchment   scale,   WaterResour.Res.,   48,   W10544,

900 doi:10.1029/2011WR011518.

901

902 Sanchez N., J. Martinez-Fernandez, A. Scaini and C. Perez-Gutierrez, "Validation of the
903 SMOS L2 Soil Moisture Data in the REMEDHUS Network (Spain)," in IEEE Transactions
904 on Geoscience and Remote Sensing, vol. 50, no. 5, pp. 1602-1611, May 2012. doi:
905 10.1109/TGRS.2012.2186971

906

907 Sánchez-Ruiz, S., Piles, M., Sánchez, N., Martínez-Fernández, J., Vall-llossera, M., &
908 Camps, A. (2014). Combining SMOS with visible and near/shortwave/thermal infrared
909 satellite data for high resolution soil moisture estimates. Journal of Hydrology, 516, 273–283.
910 https://doi.org/10.1016/j.jhydrol.2013.12.047

911

912 Schubert, M., & Boche, H. (2004). Solution of the multiuser downlink beamforming problem
913 with individual SINR constraints. IEEE Transactions on Vehicular Technology, 53(1), 18-28.

914

915 Schwank, M., Wigneron, J. P., Lopez-Baeza, E., Volksch, I., Matzler, C., & Kerr, Y. H.
916 (2012). L-band radiative properties of vine vegetation at the MELBEX III SMOS cal/val site.
917 IEEE Transactions on Geoscience and Remote Sensing, 50(5), 1587-1601.

918

919 Seneviratne, S. I., Corti, T., Davin, E. L., Hirschi, M., Jaeger, E. B., Lehner, I., ... & Teuling,
920 A. J. (2010). Investigating soil moisture–climate interactions in a changing climate: A review.
921 Earth-Science Reviews, 99(3), 125-161.

922

923 SMOS-BEC Team (2016): SMOS-BEC Ocean and Land Products Description. Technical

924 report. Available at: http://bec.icm.csic.es/doc/BEC-SMOS-0001-PD.pdf

925

926 Taylor, C. M., & Lebel, T. (1998). Observational evidence of persistent convective-scale

927 rainfall patterns. Monthly Weather Review, 126(6), 1597-1607.

928

929 Vautard, R., Yiou, P., D'andrea, F., De Noblet, N., Viovy, N., Cassou, C., ... & Fan, Y.

930 (2007). Summertime European heat and drought waves induced by wintertime Mediterranean

931 rainfall deficit. Geophysical Research Letters, 34(7).

932

933 Vidal, J.-P., E. Martin, L. Franchistéguy, M. Baillon, J.-M. Soubeyroux, A 50-year high-

934 resolution atmospheric reanalysis over France with the Safran system, Int. J. Climatol. 30

935 (2010) 1627–1644.

936

937 Wagner, W.; Dorigo, W.; de Jeu, R.; Fernandez, D.; Benveniste, J.; Haas, E.; Ertl, M. Fusion

938 of active and passive microwave observations to create an essential climate variable data

939 record on soil moisture (2012). ISPRS Ann. Photogramm. Remote Sens. Spat. Inf. Sci. 1–7,

940 315–321.

941

942 Walker, J., & Rowntree, P. R. (1977). The effect of soil moisture on circulation and rainfall in

943 a tropical model. Quarterly Journal of the Royal Meteorological Society, 103(435), 29-46.

944

945 Western, A. W., Grayson, R. B., & Blöschl, G. (2002). Scaling of soil moisture: A hydrologic

946 perspective. Annual Review of Earth and Planetary Sciences, 30(1), 149-180.

947

948 Wigneron, J. P., Calvet, J. C., Pellarin, T., Van de Griend, A. A., Berger, M., & Ferrazzoli, P.

949 (2003). Retrieving near-surface soil moisture from microwave radiometric observations:

950 current status and future plans. Remote Sensing of Environment, 85(4), 489-506.

951

952 Wigneron, J.-P., M. Schwank, E. Lopez Baeza, Y. Kerr, N. Novello, C. Millan, C. Moisy, P.

953 Richaume, A. Mialon, A. Al Bitar, F. Cabot, H. Lawrence, D. Guyon, J-C Calvet, J. P. Grant,

954 P. de Rosnay, A. Mahmoodi, S. Delwart, S. Mecklenburg (2012). First Evaluation of the

955 Simultaneous SMOS and ELBARA-II Observations in the Mediterranean Region. Remote

956 Sensing of Environment, 124, 26–37

957

958 Zampieri, M., F. D'Andrea, R. Vautard, P. Ciais, N. de Noblet-Ducoudré, and P. Yiou, 2009:

959 Hot European Summers and the Role of Soil Moisture in the Propagation of Mediterranean

960 Drought. J. Climate, 22, 4747–4758, https://doi.org/10.1175/2009JCLI2568.1

961

962

963

964

965

966

967 **Tables**

968

969 **Table 1:** Characteristics of soil moisture stations within the VAS domain.

NAME	STATION	DOMINANT VEGETATION USED FOR SIMULATIONS	TYPE OF VEGETATION	SAND	SILT	CLAY	ALTITUDE (m)	ANNUAL MEAN TEMPERATURE (°C)	ANNUAL MEAN PRECIPITATION (mm)
Melbex_I		Schrub	Schrub	0,47	0,38	0,15	849	(12-14)	451
Nicolas		Vineyard	Schrub/ Vineyard	0,47	0,35	0,18	859		
La Cubera		Vineyard	Vineyard	0,45	0,35	0,20	762		
Ezpeleta		Olive tree	Olive tree	0,44	0,39	0,17	781		
VAS		Vineyard	Vineyard	0,46	0,37	0,17	804		
Melbex_II		Vineyard	Vine stump/ Vine row	0,45	0,29	0,26	797		

970

971

972

973

974

975

976

977

978

979

980

981

982

983

984

43

985

986

Table 2: Number of days (percentage) in which the SMOS (ascendant and descendent
swaths) coverage is higher than 50 %.

989

LEVEL SMOS	SEPTEMBER		OCTOBER		NOVEMBER		SON	
	days	%	days	%	days	%	days	%
L4$^{2.0}$ (~1km)	10	34	9	31	9	31	28	32
L4$^{3.0}$ (~1km)	23	74	29	90	30	100	82	92
L2 (~15km)	20	67	28	90	28	93	76	83
L3 (~25km)	22	73	29	93	29	96	80	88

990

991

992

993

994

995

996

997

998

999

1000

1001

1002

1003

1004

1005

1006

1007

1008

1009

1010 **Table 3:** Statistics of the comparions between SMOS-L2 and SMOS-L4$^{3.0}$ soil moisture
1011 versus ground-based measurements in the VAS network (the area covering the ground-
1012 based network has been called OBS, Figure 1). SMOS descendent orbits are selected for
1013 the comparison. Characteristics of the individual stations are given in Table 1. The acronyms
1014 for the names of the stations are as follows: (M-I: Melbex_I, M_II: Melbex_II, VAS: VAS, NIC:
1015 Nicolas, EZ: Ezpeleta, LC: La Cubera). The period December 2011 to December 2012 is
1016 evaluated. The seasonal analysis follows the hydrological cycle. OBS stands for the average
1017 of (i) SMOS-L2 and/or SMOS-L4$^{3.0}$ soil moisture values within the 10x10 km^2 where the
1018 ground-based network is placed, and (ii) in the case of the in situ observations it refers to the
1019 mean of all stations. In Table (a) a seasonal comparison between the mean of all in situ
1020 stations and the corresponding mean of SMOS-L2 and/or SMOS-L4$^{3.0}$ soil moisture values
1021 within the 10x10 km^2 area. In (b) SMOS-L2 and SMOS-L4$^{3.0}$ soil moisture observations are
1022 compared to point-like ground measurements using the closest grid point. The column on the
1023 right shows the mean of all stations

1024

1025 (a)

OBS vs SMOS-L2	Slope	R2	Bias	CRMS	OBS vs SMOS-L4$^{3.0}$	Slope	R2	Bias	CRMS
DJF	1.1	0.5	-0.09	0.03	DJF	1.0	0.7	-0.03	0.04
MAM	0.6	0.2	-0.07	0.03	MAM	0.6	0.4	-0.03	0.03
JJA	0.3	0.01	-0.02	0.03	JJA	0.1	0.01	-0.003	0.03
SON	1.1	0.8	-0.02	0.04	SON	0.8	0.7	-0.003	0.04

1026

1027 (b)

SMOSL2 vs SMOSL4$^{3.0}$	M-I	M-II	VAS	NIC	EZ	LC	OBS (mean all stations)
DJF							
Slope	0.17/-0.04	1.0/1.7	1.6/2.3	1.1/1.7	0.8/0.9	0.9/1.7	1.1/0.6
R2	0.02/0.01	0.6/0.5	0.8/0.5	0.9/0.7	0.5/0.2	0.7/0.7	0.5/0.7
MB	-0.03/-0.08	-0.08/-0.14	0.01/-0.04	0.006/-0.05	0.03/-0.02	0.004/-0.05	-0.09/-0.03
CRMSD	0.04/0.03	0.03/0.02	0.04/0.03	0.03/0.03	0.04/0.03	0.04/0.03	0.03/0.04
MAM							
Slope	0.4/0.36	0.6/0.4	0.8/0.6	0.6/0.8	0.5/0.3	0.9/0.7	0.6/0.6
R2	0.2/0.08	0.3/0.04	0.5/0.15	0.9/0.5	0.3/0.14	0.4/0.2	0.2/0.4
MB	-0.04/-0.08	-0.08/-0.11	0.005/-0.03	0.003/-0.03	0.02/-0.02	-0.02/-0.05	-0.07/-0.03
CRMSD	0.03/0.03	0.03/0.03	0.03/0.03	0.03/0.03	0.04/0.03	0.03/0.03	0.03/0.03
JJA							
Slope	0.26/0.38	0.3/0.4	0.02/0.15	0.1/0.3	0.08/-0.04	0.05/0.06	0.3/0.1
R2	0.02/0.01	0.04/0.005	0.001/0.002	0.8/0.17	0.003/0.012	0.01/0.003	0.01/0.01
MB	-0.01/-0.03	-0.04/-0.05	0.03/0.012	0.01/0.002	0.05/0.04	0.03/0.02	-0.02/-0.003
CRMSD	0.03/0.03	0.03/0.03	0.03/0.03	0.03/0.03	0.03/0.03	0.03/0.03	0.03/0.03
SON							
Slope	0.69/1.06	0.9/1.3	1.2/1.7	0.8/1.2	0.7/1.1	0.8/1.3	1.1/0.8
R2	0.5/0.6	0.6/0.6	0.7/0.8	0.9/0.7	0.8/0.7	0.8/0.7	0.8/0.07
MB	-0.02/-0.04	-0.03/-0.05	0.04/-0.03	0.03/0.006	0.03/0.01	0.04/0.02	-0.02/-0.003
CRMSD	0.04/0.04	0.04/0.04	0.04/0.04	0.04/0.04	0.04/0.04	0.04/0.04	0.04/0.04

1028

1029

1030

1031

1032

1033

1034

1035

Table 4: Statistics of daily areal averages of ground-based SSM measurements in the OBS area versus point-like SURFEX(ISBA) simulations at the same sites. The acronyms for the names of the stations are as described in Table 3.

1039

	M-I	M-II	VAS	NIC	EZ	LC	OBS
All period							
Slope	0.9	1.3	0.9	0.7	1.0	0.9	1.0
R2	0.8	0.8	0.8	0.8	0.8	0.7	0.9
MB	0.004	-0.012	0.011	0.006	0.02	0.006	0.005
CRMSD	0.02	0.02	0.02	0.02	0.01	0.02	0.02
DJF							
Slope	0.2	1.3	0.8	1.2	1.2	1.1	1.1
R2	0.03	0.4	0.4	0.7	0.7	0.5	0.6
MB	0.01	-0.03	0.02	0.03	0.02	0.03	0.01
CRMSD	0.04	0.05	0.03	0.04	0.03	0.03	0.04
MAM							
Slope	0.8	1.0	1.0	0.7	0.8	0.7	0.9
R2	0.5	0.4	0.6	0.4	0.6	0.5	0.6
MB	0.002	-0.02	0	0.01	0.01	-0.02	-0.004
CRMSD	0.04	0.02	0.03	0.04	0.03	0.04	0.04
JJA							
Slope	0.4	0.8	1.6	3	1.6	2	1.5
R2	0.7	0.8	0.7	0.5	0.7	0.6	0.8
MB	0.004	0.01	0.01	-0.02	0.02	0.005	0.005
CRMSD	0.04	0.02	0.03	0.04	0.03	0.04	0.04
SON							
Slope	0.9	1.1	0.9	0.8	1.0	1.1	1.0
R2	0.8	0.8	0.8	0.9	0.9	0.8	0.9
MB	0.002	0	0.01	0	0.02	0.01	0.006
CRMSD	0.04	0.006	0.03	0.04	0.04	0.03	0.04

1040

1041

1042

1043

1044

1045

1046

1047

1048

1049

1050

1051

1052 **Figures**

1053
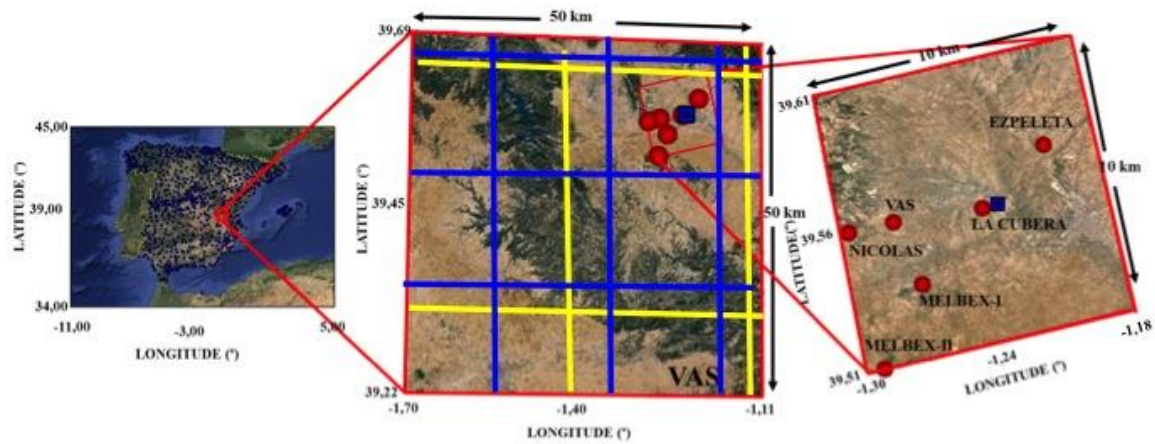
1054

1055

1056 **Figure 1:** Area of investigation and orography. Location of rain gauges from AEMET
1057 (Meteorological Service of Spain) is shown over the Iberian Peninsula (blue square dots).
1058 The positions of the soil moisture network stations within the 10x10 km^2 (OBS area) in the
1059 Valencia Anchor Station (VAS; 50x50 km^2) area are indicated by red circles.

1060

1061

1062

1063

1064

1065

1066

1067

1068

1069

1070

1071
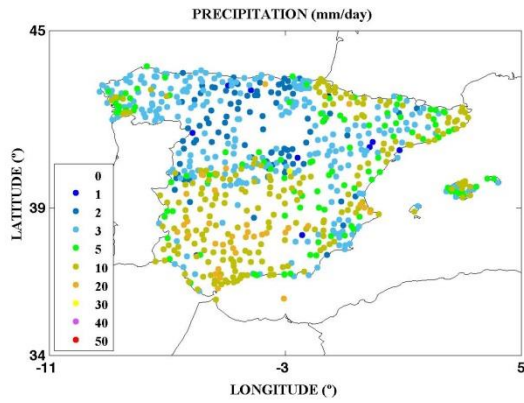
1072
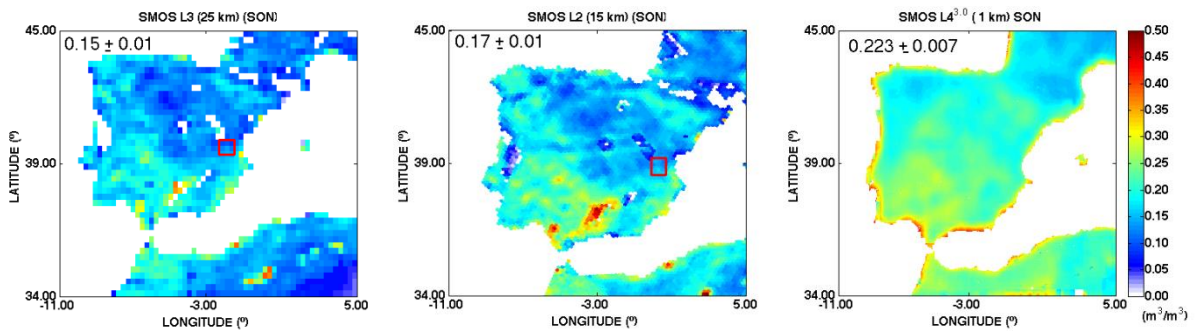
1073
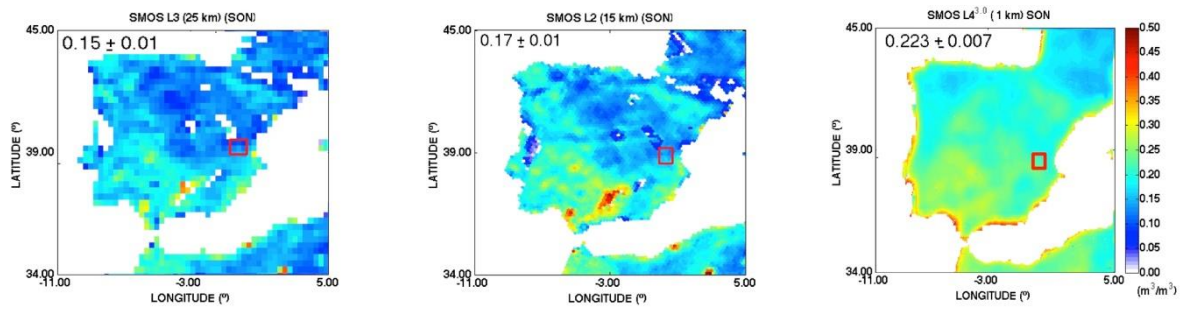
1074

1075

Figure 2: (a) Spatial distribution of precipitation over the Iberian Peninsula from the network of rain gauges of AEMET. The period of September to November (SON) 2012 is shown. (b) Spatial distribution of SMOS-derived soil moisture over the Iberian Peninsula (merged product: ascending and descending orbits, days with areal coverage higher than 50 % are considered).

1081

1082

1083

1084

1085

1086

1087

1088

1089

1090

1091

1092

1093

1094

1095

1096 **Figure 3:** SMOS-derived SSM products comparison from different operational levels over the
1097 Iberian Peninsula.
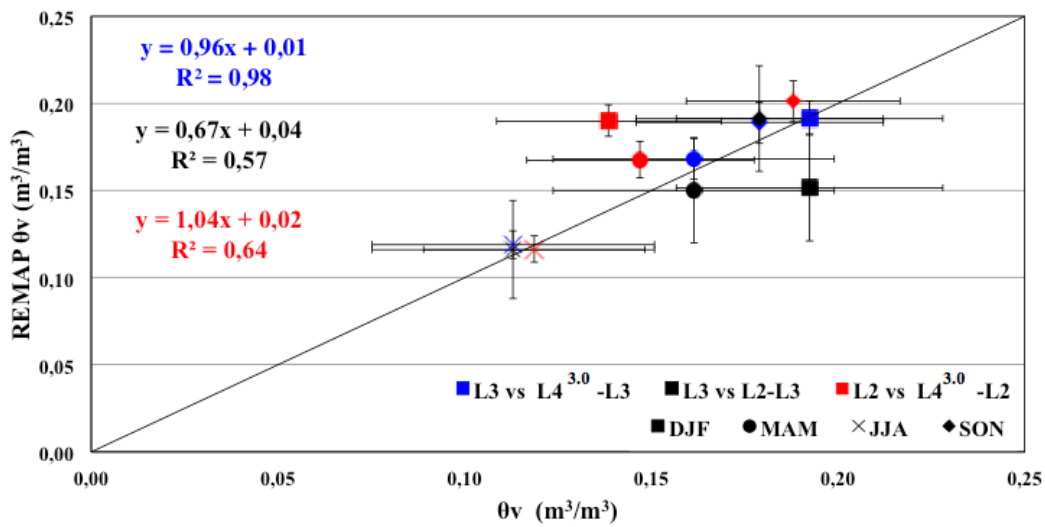
1098

1099

1100

1101

1102

1103

1104

1105

1106

1107

1108

1109

1110   (a)
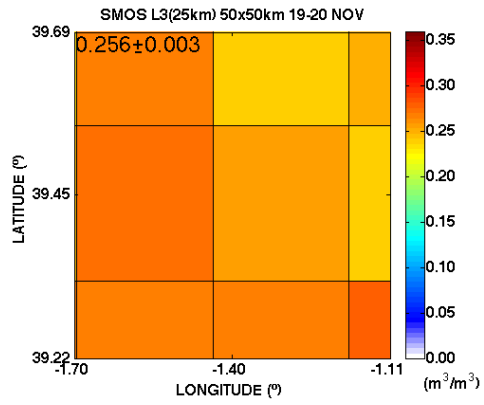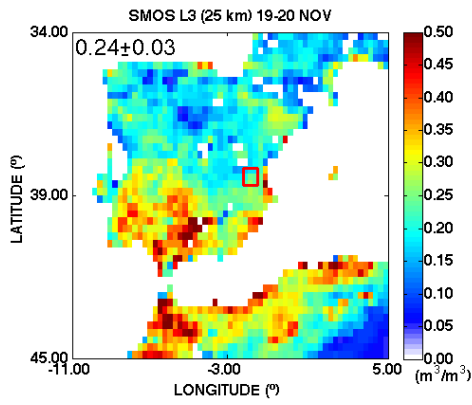
1111
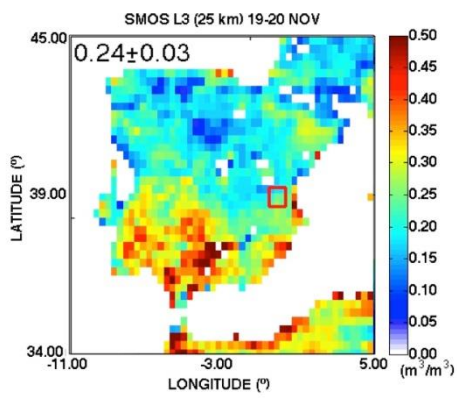
1112

1113

1114

1115

1116

1117

1118

1119

1120

1121

1122

1123

1124

1125

1126

1127

1128   (b)
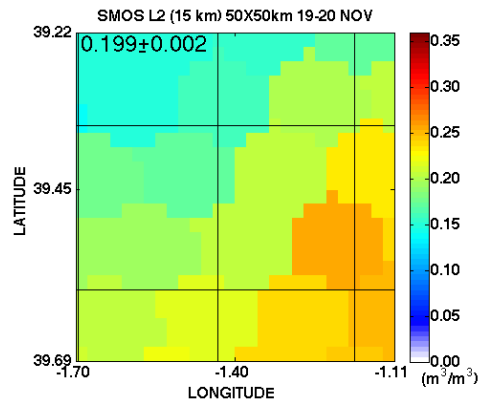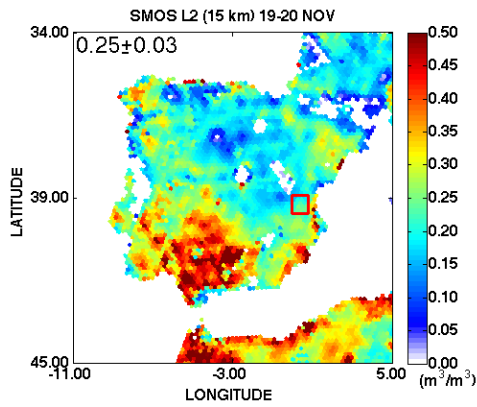
1129
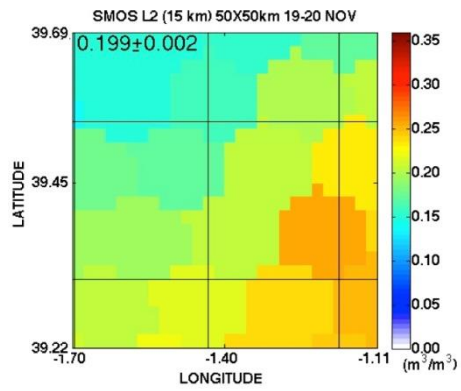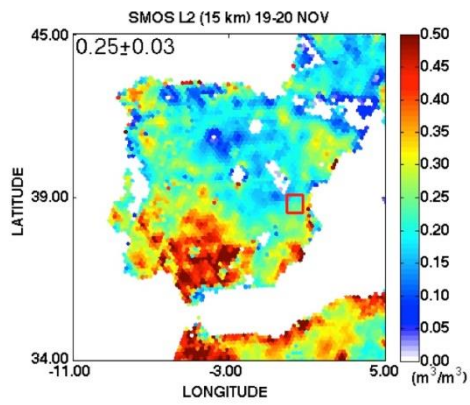
1130
1131
1132
1133
1134
1135
1136
1137
1138
1139
1140
1141
1142
1143
1144
1145
1146
1147
1148
1149
1150
1151
1152
1153
1154
1155
1156
1157
1158
1159
1160
1161
1162

1163

1164

1165   (c)
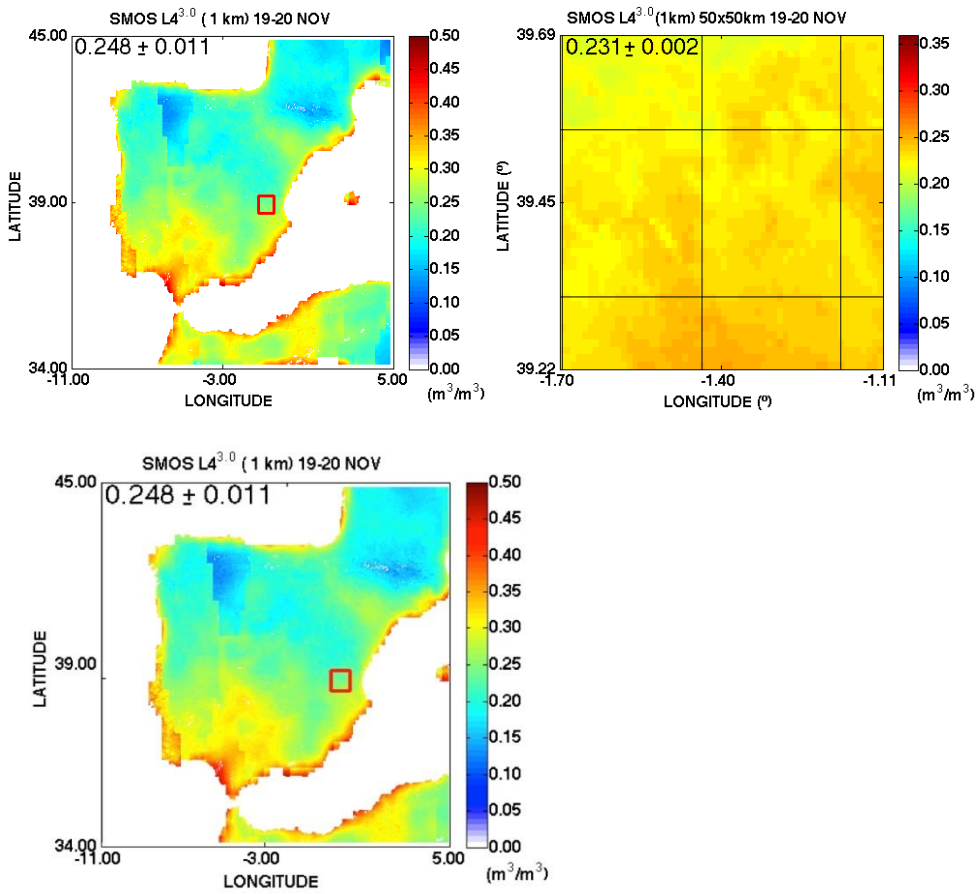
1166

1167

1168

1169   **Figure 4:** Spatial distribution of SMOS-derived soil moisture (merged product: ascending and
1170   descending orbits are considered) over the Iberian Peninsula (left) and the VAS (right) as a
1171   mean for the 19-20 November of 2012 (a) SMOS-L3 (~25 km), (b) SMOS-L2 (~15 km), (c)
1172   SMOS-L4$^{3.0}$ (~1 km). White empty pixels in (a) and (b) are indicative of a lack of data. Please
1173   be aware of the different colour scale used for the IP and VAS.

1174

1175

1176

1177

1178

1179

1180

1181

1182

1183

1184   (a)
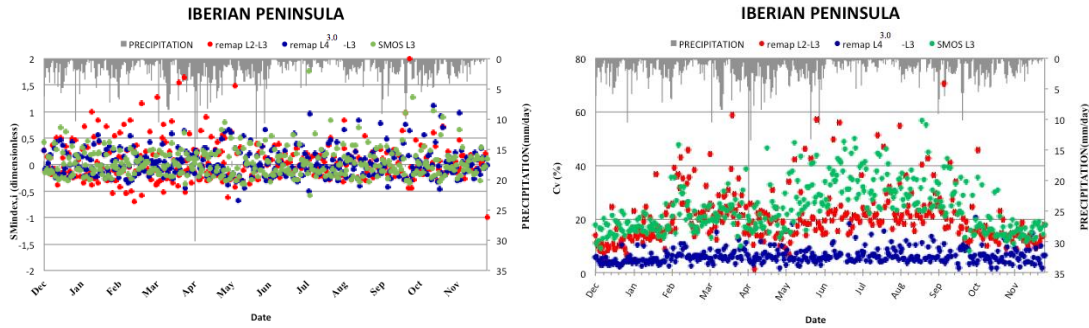
1185

1186

1187   (b)
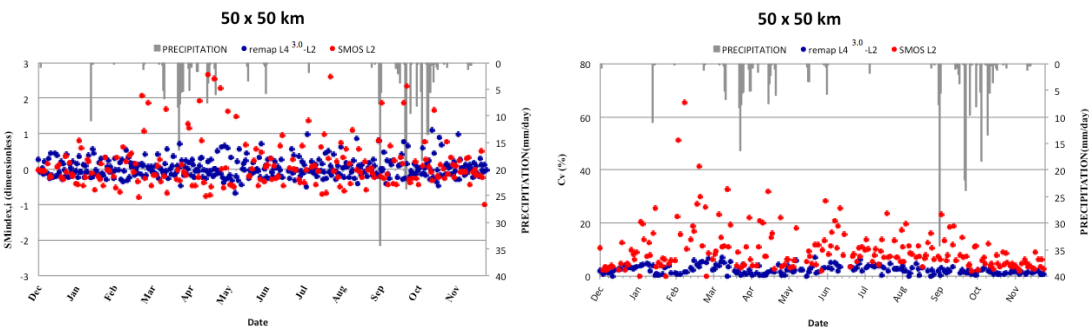
1188

1189   (c)
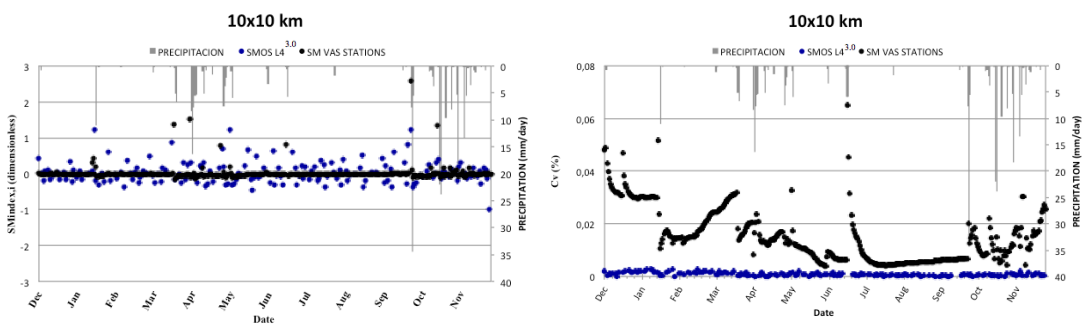
1190

Figure 5: Averaged SMOS products and averaged ground-based observations of soil
moisture evolution over the Iberian Peninsula (IP; top), the VAS area (centre), and the OBS
area (bottom). Descending orbits are used. Precipitation from AEMET rain gauges on top.
Left) Soil moisture daily index ($\Theta_{v\ index,i}$; dimensionless) and right) Coefficient of variation (Cv,
%).

1196

1197

1198   (a)

IBERIAN PENINSULA
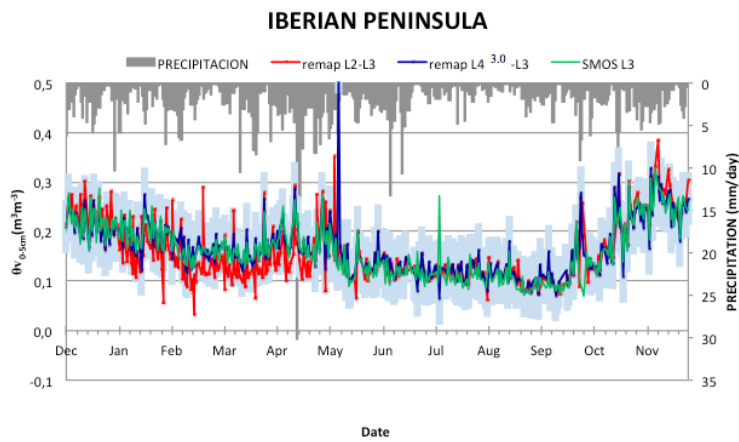
1199

1200   (b)
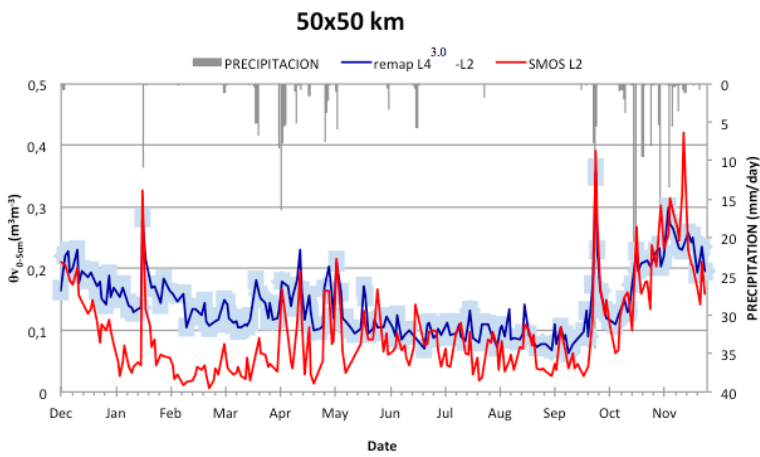
50x50 km

1201

1202   (c)
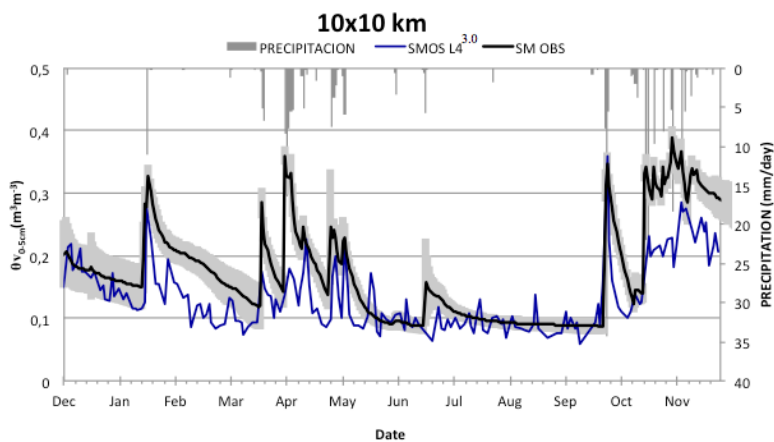
10x10 km

1203

1204   **Figure 6:** Temporal evolution of surface soil moisture time series averaged over the Iberian
1205   Peninsula (top), the VAS area (50 x 50 km^2; centre) and the OBS area (10 x 10 km^2; bottom).
1206   SMOS afternoon orbits are considered. Daily mean precipitation from the AEMET stations is

1207   shown on top of each plot. SMOS and remapped SMOS products are indicated in the plots.
1208   Shaded areas show standard deviations, respectively.

1209

1210

1211

1212

1213

1214

1215

1216

1217

1218

1219

1220

1221

1222

1223

1224

1225

1226

1227

1228

1229

1230

1231

1232

1233

1234

1235   (a)
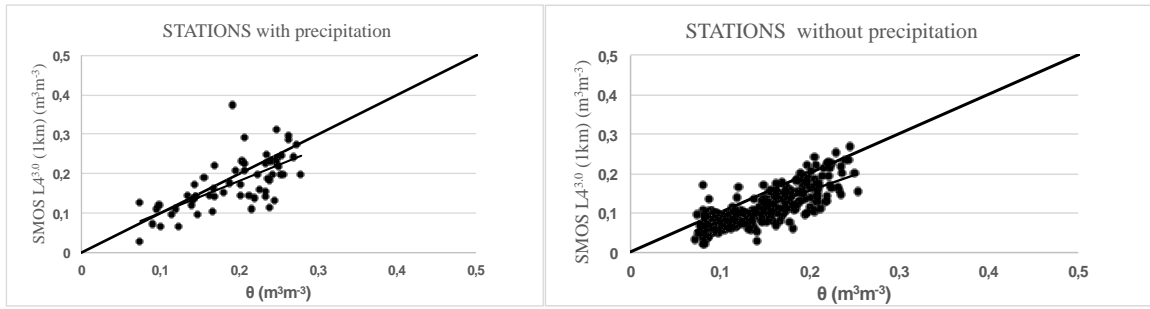
1236

1237

1238 (b)
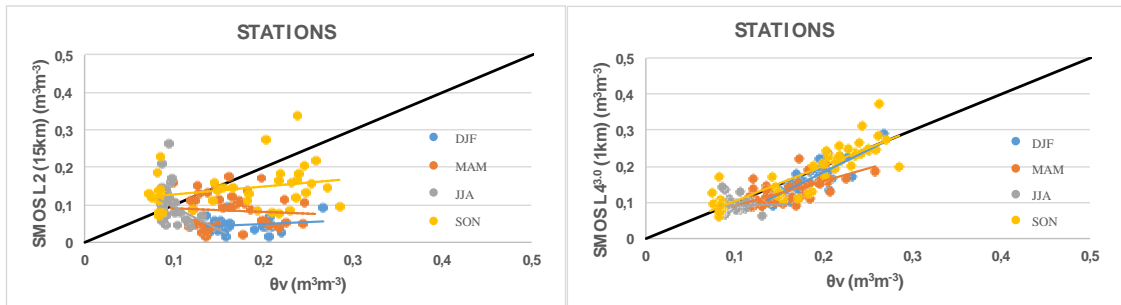
1239

1240

1241 (c)
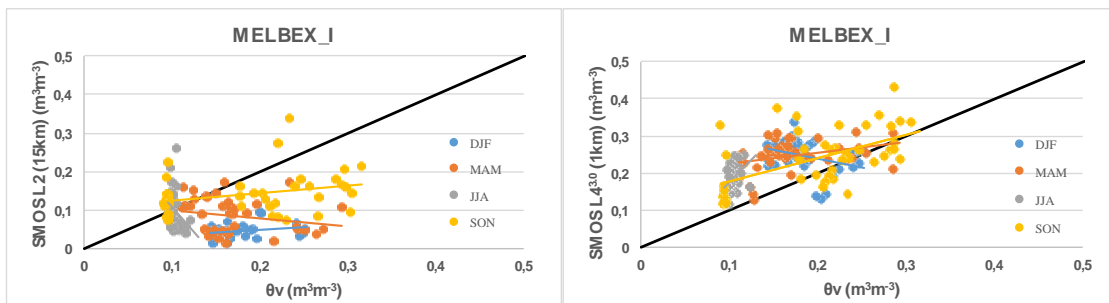
1243

1244

1245 **Figure 7:** Results of the seasonal analysis for the hydrological year starting in December
1246 2011. Scatter plots of (a) SMOS-L4[3.0] SSM (ascending and descending orbits) versus
1247 averaged 10x10 km^2 in situ soil moisture measurements (left) for days with precipitation, and
1248 (right) and without precipitation (< 1 mm /d). (b) SMOS-L2 and SMOS-L4[3.0] SSM (descending
1249 orbits) versus averaged 10x10 km^2 in situ soil moisture measurements. (c) SMOS-L2 and
1250 SMOS-L4[3.0] SSM (descending orbits) versus point-like ground measurements from
1251 MELBEX_I station, using the closest grid point. Segments are linear fit of seasonal data (3
1252 months data). Statistics for individual comparisons at all stations are summarized in Table 3.

1253

1254   (a)
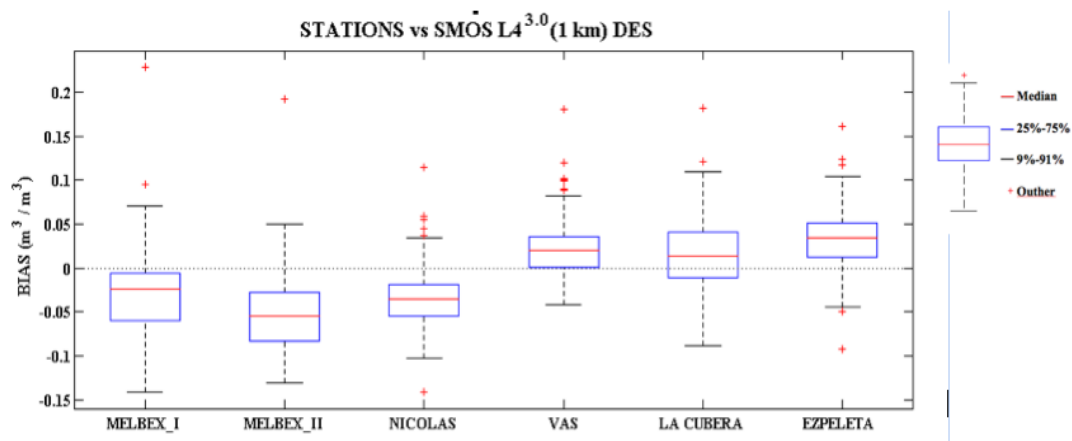
1255

1256

1257   (b)
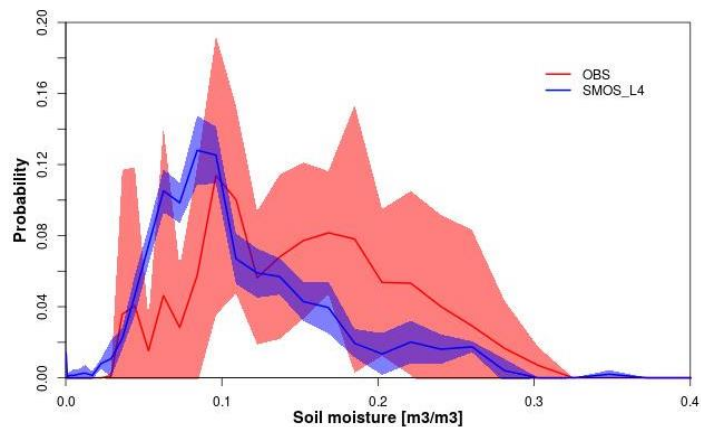
1258

1259   **Figure 8:** (a) Box plot of the comparison between point-like ground measurements at all
1260   stations over the VAS area and closest SMOS-L4[3.0] SSM data. (b) Probability distribution
1261   funtion (PDF) of SSM from in situ observations and SMOS- L4[3.0] SSM measurements. The
1262   standard deviations are indicated with shaded areas. Full lines represent the mean over all
1263   ground stations and over the 10 x 10 km^2 of the OBS area in VAS where the in SSM network
1264   is located.

1265

1266

1267

1268

1269

1270

1271
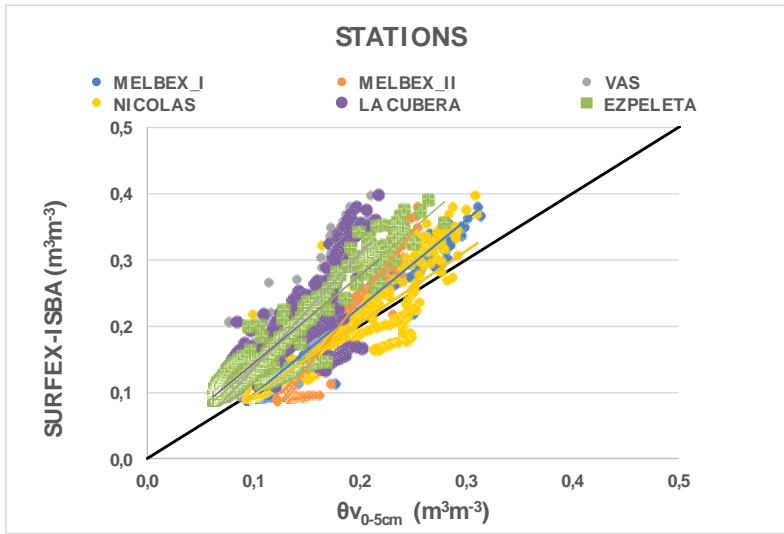
1272

1273

1274 **Figure 9**: Scatter plot of temporal mean (over the whole simulation period) SSM ground
1275 measurements versus SURFEX(ISBA) simulations (realistic initial scenario; REAL-I) at all
1276 stations. Statistics for all stations using the REAL-I initial scenario are presented in Table 4.

1277

1278

1279

1280

1281

1282

1283
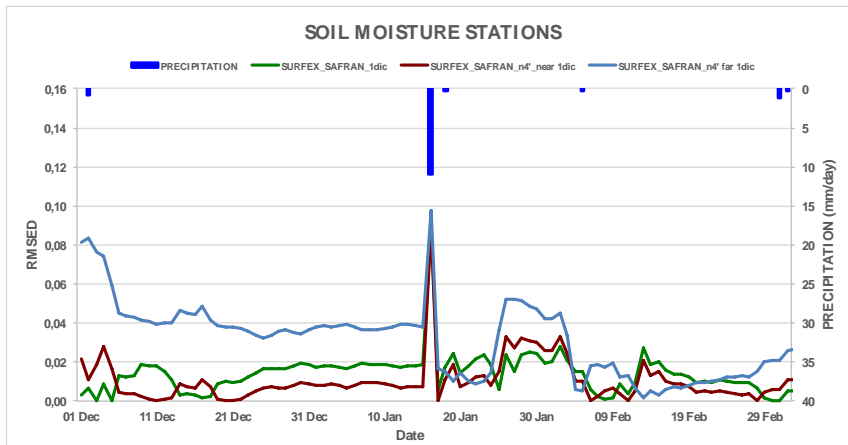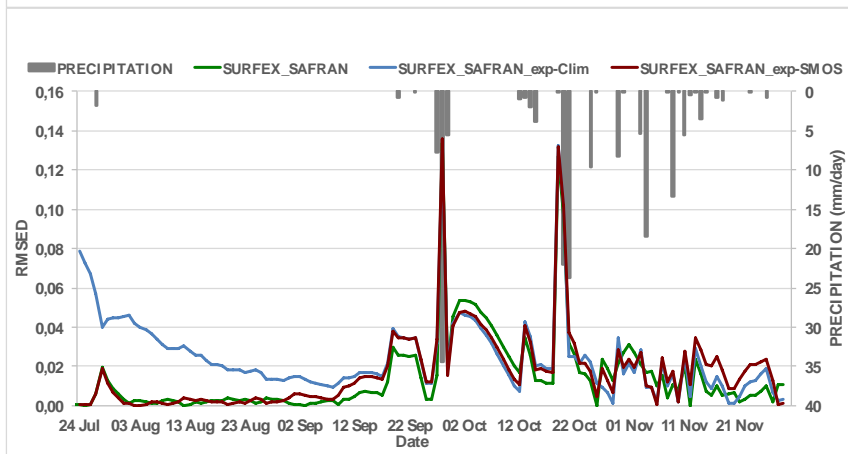
1284

1285

1286

1287

1288

1289

1290

1291

1292

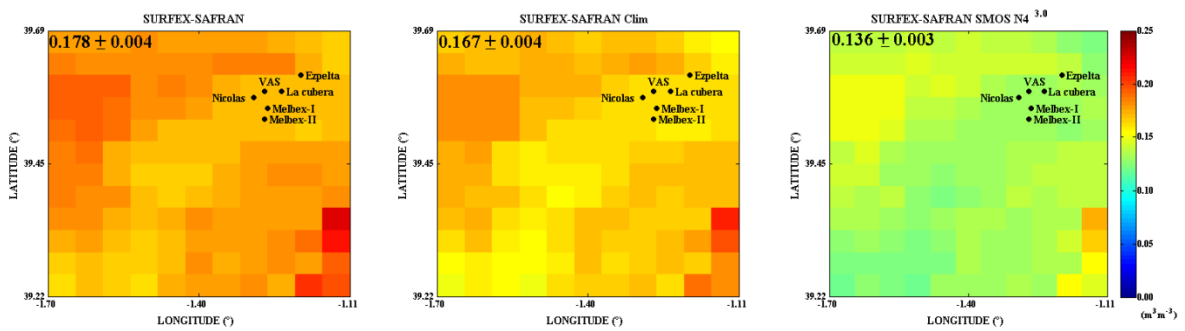1293

1294   (a)

1295

1296
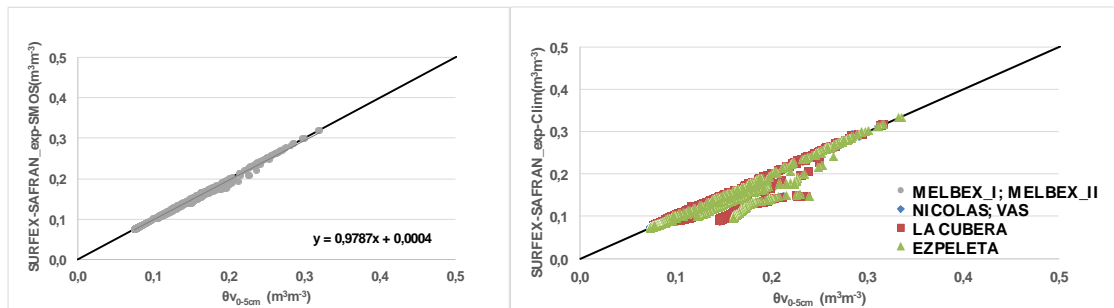
1297

1298   (b)

1299

1300

1301

1302

1303

1304

1305

1306 (c)

1307

1308

1309

1310

1311 **Figure 10:** (a) RMSD for the daily mean SSM from the three $\mathrm{SURFEX(ISBA)}$ simulations
1312 with perturbed initial SSM scenarious (details in section 4.3.2). (b) Spatial distribution of
1313 mean SSM for the winter simulation (a, left) for the 3 simulations. (c) Scatter plot depicting
1314 the compariosn between in situ SSM observations and SURFEX-SAFRAN-SMOSL4$^{3.0}$
1315 simulations, as a mean over all stations (left) and for each of the stations (right).

1316

1317

1318

1319